END

DATE
FILMED
5-88

MICROCOPY RESOLUTION TEST CHART

NATIONAL BUREAU OF STANDARDS 1963 A

AFGL-TR-87-0205

Design, Fabricate, Calibrate, Test
and Deliver Two Satellite Electron
Flux Detectors

AD-A190 799

Jean L. Hunerwadel
Bach Sellers
Frederick A. Hanser

Panametrics, Inc.
221 Crescent Street
Waltham, MA 02254

June 1987

Final Report

24 September 1979 - 20 August 1986

APPROVED FOR PUBLIC RELEASE; DISTRIBUTION UNLIMITED

88 1 27 171

"This technical report has been reviewed and is approved for publication"

_____
(Signature)
DAVID A. HARDY
Contract Manager

_____
(Signature)
E. G. MULLEN
Branch Chief

FOR THE COMMANDER

_____
(Signature)
R. C. SAGALYN
Division Director

SECURITY CLASSIFICATION OF THIS PAGE (When Data Entered)

REPORT DOCUMENTATION PAGE		READ INSTRUCTIONS BEFORE COMPLETING FORM
1. REPORT NUMBER AFGL-TR-87-0205	2. GOVT ACCESSION NO.	3. RECIPIENT'S CATALOG NUMBER
4. TITLE (and Subtitle) DESIGN, FABRICATE, CALIBRATE, TEST AND DELIVER TWO SATELLITE ELECTRON FLUX DETECTORS		5. TYPE OF REPORT & PERIOD COVERED Final Report 24 Sept 79 to 20 Aug 86
		6. PERFORMING ORG. REPORT NUMBER
7. AUTHOR(s) Jean L. Hunerwadel Bach Sellers Frederick A. Hanser		8. CONTRACT OR GRANT NUMBER(s) F19628-79-C-0175
9. PERFORMING ORGANIZATION NAME AND ADDRESS Panametrics, Inc. 221 Crescent Street Waltham, MA 02254		10. PROGRAM ELEMENT, PROJECT, TASK AREA & WORK UNIT NUMBERS 62101F 760112AE
11. CONTROLLING OFFICE NAME AND ADDRESS Air Force Geophysics Laboratory Hanscom AFB, MA 01731 Contract Manager: David Hardy/PHG		12. REPORT DATE June 1987
		13. NUMBER OF PAGES 58
14. MONITORING AGENCY NAME & ADDRESS(if different from Controlling Office) DCASMA, Boston 666 Summer Street Boston, MA 02210		15. SECURITY CLASS. (of this report) UNCLASSIFIED
		15a. DECLASSIFICATION DOWNGRADING SCHEDULE

16. DISTRIBUTION STATEMENT (of this Report)

Approved for public release, distribution unlimited.

17. DISTRIBUTION STATEMENT (of the abstract entered in Block 20, if different from Report)

18. SUPPLEMENTARY NOTES

19. KEY WORDS (Continue on reverse side if necessary and identify by block number)

High Energy Electron Analyzer, Very Low Background High Energy Electron Spectrometer, Electron and Proton Detectors, Fast Triple Coincidence and Anticoincidence Electron Spectrum Analysis, CRRES Satellite Instrumentation

20. ABSTRACT (Continue on reverse side if necessary and identify by block number)

A satellite borne High Energy Electron Analyzer has been designed to measure electrons in the range of 1 MeV to 10 MeV. Very low background from omnidirectional charged particles is achieved with two Solid State Detectors and a BGO scintillator crystal arranged in a telescope unit and with the requirement of a triple coincidence of electrons in the measurement range. Ten energy bins are provided by the BGO over this range. Additionally, electron singles above 10 MeV and proton singles above 15.7

DD FORM 1473 EDITION OF 1 NOV 65 IS OBSOLETE

SECURITY CLASSIFICATION OF THIS PAGE (When Data Entered)

MeV are measured by the BGO crystal. The Solid State Detectors also provide measurements for proton singles from 4.1 MeV to 269 MeV. The background is further reduced by a plastic scintillator, surrounding the BGO, and placed into anticoincidence with the electron measurement. A complete electron energy spectrum plus singles measurement is generated every .512 seconds. The serial digital data output contains 264 bits from 22 counters. The higher count rates from 3.5 to 1000 kcps are accommodated with compression counters while the lower count rates are accumulated in straight ripple counters. Three different coincidence requirements (Front SSD coincidence, Back SSD coincidence, Shield anticoincidence) are selectable by ground command. A serial digital command is available to control the BGO photomultiplier high voltage. Two instruments have been fabricated, tested and calibrated. The first of these has been integrated on the CRRES satellite and is currently undergoing spacecraft testing at BASD.

Accession For	
NTIS GRA&I	☑
DTIC TAB	☐
Unannounced	☐
Justification	
By	
Distribution/	
Availability Codes	
Dist	Avail and/or Special
A-1	

TABLE OF CONTENTS

LIST OF ILLUSTRATIONS

LIST OF TABLES

1.0 INTRODUCTION

The design of a High Energy Electron Analyzer (also referred to as Electron Fluxmeter) described in this report is a new approach to the difficult problem of low electron flux measurements in the energy range 1 to 10 MeV. Previously flown instruments succeeded in making electron flux measurements up to about 5 MeV. At energies above that range, measurements were generally rendered useless by background due to energetic protons (trapped or cosmic rays) or due to electron-induced bremsstrahlung.

This background problem is illustrated by the Los Alamos Scientific Laboratory (LASL) energetic electron detector, called EDGE (Electron and Delayed Gamma Experiment), flown on DMSP satellites. It achieved useful electron spectra up to about 8 MeV. However, these results could only be obtained, especially at the higher energies, by subtracting the cosmic ray background from the received data. This means the 8 MeV range was not achieved in situ, but by data analysis, and the subtraction-process statistics severely affected the measurement.

The basic fluxmeter design described here in Section 2 employs a coincidence telescope, and pulse height analysis of the BGO signals in terms of incident electron energy. The difficulty of high background due to corner cutting protons and cosmic rays is mostly overcome with the fluxmeter design, which includes an anticoincidence shield. Placing the signals from this shield in anticoincidence with the telescope signals effectively guards against corner cutting protons and hence results in lower background.

The low background is further reduced by the use of two SSD's in the telescope and by employing fast triple coincidence and anticoincidence. The desirable features of the design are: much improved energy resolution (10 energy bins), photomultiplier gain control by ground command, three in-flight calibration modes, separation of high and low energy electrons for improved flux measurements at the higher energies, and use of two solid state detectors (SSD's) in the telescope in order to reduce accidental coincidences to an extremely low value. The gain control of the photomultiplier eliminates the need to correct the data for temperature variations and aging of that detector. Proper operation of each detector in the telescope and the plastic shield is verified by means of the 3 calibration modes in conjunction with a calibration source, which is an integral part of the instrument. The beta source is useful for evaluation of in-orbit performance of the SSD's and BGO during periods of low activity.

In summary the design provides the capability to make in-situ high energy electron measurements and proton flux determinations from SSD, BGO and shield singles, accumulated in separate counters.

2.0 GENERAL INSTRUMENT DESIGN

2.1 Electron and Proton Detection

The concept is that of a semiconductor telescope in coincidence with a BGO scintillator and into anticoincidence with a plastic scintillator surrounding the BGO. The plastic detector effectively reduces most of the energetic proton contamination. A system having very low background is achieved when two solid state detectors (SSD's) in the telescope, form a triple coincidence with the BGO output, and when the coincidence pulses are of very short duration (fast coincidence).

This single scintillation crystal detects and measures the energy of electrons between 1 and 10 MeV. A cross sectional view of the sensor, which contains the BGO, the two SSD's, the plastic detector, three photomultipliers and associated electronics, is shown in Fig. 2.1.

In general, protons $\lesssim$ 100 MeV in the aperture are rejected by their energy loss in the solid state detectors; use of two detectors considerably increases the reliability of this approach. Protons above about 30 MeV energy can be rejected simply by their very large energy loss in the BGO crystal. As a consequence, there is a region between about 30 and 100 MeV where in-aperture protons are rejected by two different mechanisms. The omni-directional shielding is effective up to 140 MeV for protons and to > 20 MeV for electrons. Particles sufficiently energetic to penetrate this shielding will be rejected by the anticoincidence detector. A heavy tungsten shield and tungsten collimators are used to reduce the effects of bremsstrahlung. Generation of bremsstrahlung in the sensor housing itself is minimized by use of magnesium, which stops electrons $\lesssim$ 10 MeV near the crystal assembly. The tungsten collimators also define sharp transmission edges on the solid state detectors. Thus, abnormally low energy losses produced by protons passing through the outer, thin depletion region of the detector are minimized - such low energy losses would cause the protons to be misidentified as electrons.

A beryllium shield 0.006" thick is used to stop electrons below about 0.14 MeV. The solid state semiconductor detectors to be used are 700 μm thick, having 100 and 50 mm^2 area, respectively. They are Ortec models B-018-100-700 and B-018-50-700. The detector noise for electrons is 10 keV. This choice of detector thickness represents a compromise between 1000 μm detectors (which would not permit passage of 1 MeV electrons into the BGO crystal), and 500 μm detectors - for which the energy loss by 10 MeV electrons is not sufficiently large to guarantee no noise difficulty problems on a long-term basis.

We have used stopping power date for electrons (Refs. 2.1 and 2.2) and protons (ref. 2.3) to calculate the <u>average</u> energy deposited in each of the detectors, as shown in Figs. 2.2 and 2.3.

2
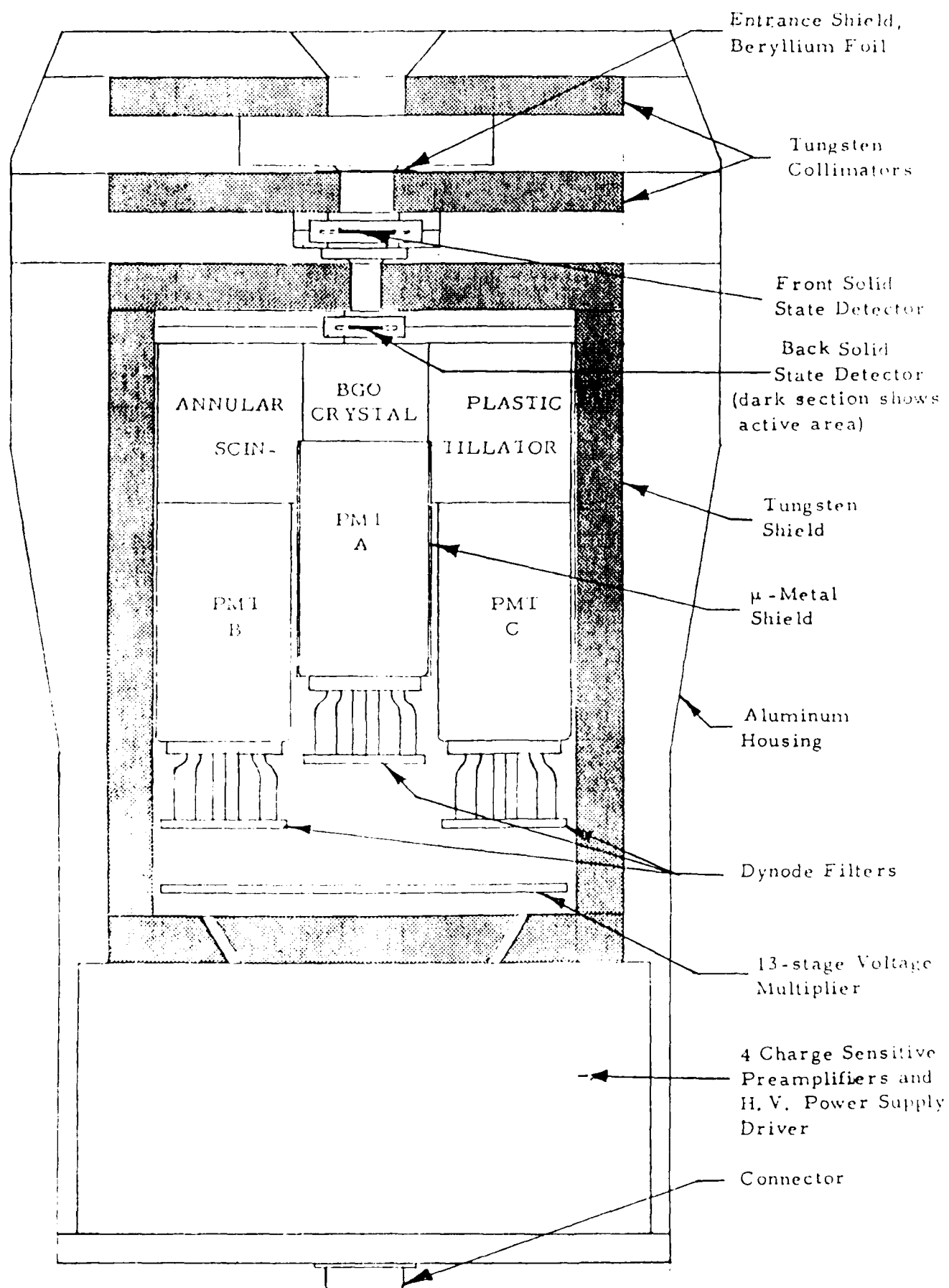
Figure 2.1 Cross Section of Energetic Electron Fluxmeter

3

Labels in figure:
Entrance Shield, Beryllium Foil
Tungsten Collimators
Front Solid State Detector
Back Solid State Detector (dark section shows active area)
Tungsten Shield
μ-Metal Shield
Aluminum Housing
Dynode Filters
13-stage Voltage Multiplier
4 Charge Sensitive Preamplifiers and H.V. Power Supply Driver
Connector

ANNULAR SCIN-TILLATOR
BGO CRYSTAL
PLASTIC TILLATOR
PMT A
PMT B
PMT C

The thresholds S_0 and S_1 in Fig. 2.2 form the energy deposition window W_1 to be applied for energetic electrons (3-10 MeV). The window must be widened somewhat for lower energy electrons (1-3 MeV); thus the threshold S_2 is used with S_0 to define the window W_2 for those electrons. These windows are used to define coincidences with each other and with the BGO crystal output.

Figure 2.3 shows the energy deposited in the BGO crystal. It is clear from the figure that all in-aperture penetrating protons $\gtrsim$ 19 MeV can be separated simply by use of the < L10 threshold. Penetrating protons can pass through the edge of the BGO crystal and produce a lower energy deposition, but in this case there would also be a plastic shield scintillator veto pulse generated and further, there would have been no coincidence in the SSD telescope. The BGO output is analyzed into ten energy bins defined by the thresholds LL to L10. We have used ten bins because we believe it will provide the spectral resolution necessary to provide the required separation of AE 17 HI and LO.

The proton distributions are skewed toward large energy losses, as is the case for electrons. Here that is of considerable benefit, since it tends to reduce the probability that a proton will lose <u>much</u> less than the average in Fig. 2.2. Such a loss could cause it to appear in the electron window even if its average energy loss were above the appropriate threshold S_1 and S_2. The use of two detectors causes this probability to be much reduced, since it would have to occur in each detector. Additionally, protons above about 30 MeV will produce a very large (>> 10 MeV) pulse in the BGO crystal. Use of both the large BGO energy loss and the thresholds S_1 and S_2 in the SSD's guarantees extreme immunity against analysis of in-aperture protons that pass through the SSD's and either into or through the BGO crystal.

Similar statements can be made regarding the possibility of analyzing bremsstrahlung. The probability of a true coincidence is exceedingly small.

2.2 Geometric Factors and Count Rates

The geometric factors of the four particle detectors consist of two components: the in-aperture telescope response and the out-of-aperture omnidirectional response. The various geometric factors are given in Table 2.1. The approximate W (tungsten) shielding equivalent for the omnidirectional responses is based on the design of Fig. 2.1 and is a conservative estimate. Other materials (magnesium, plastic scintillator) have been converted into W (tungsten) equivalent by using proton stopping power ratios for the 100 MeV region.

The detailed particle response characteristics for each detector by itself (no coincidence requirements) are given in Table 2.2. The 22 channels listed in Table 2.2 provide a complete set of data, which allow verification of proper instrument

4
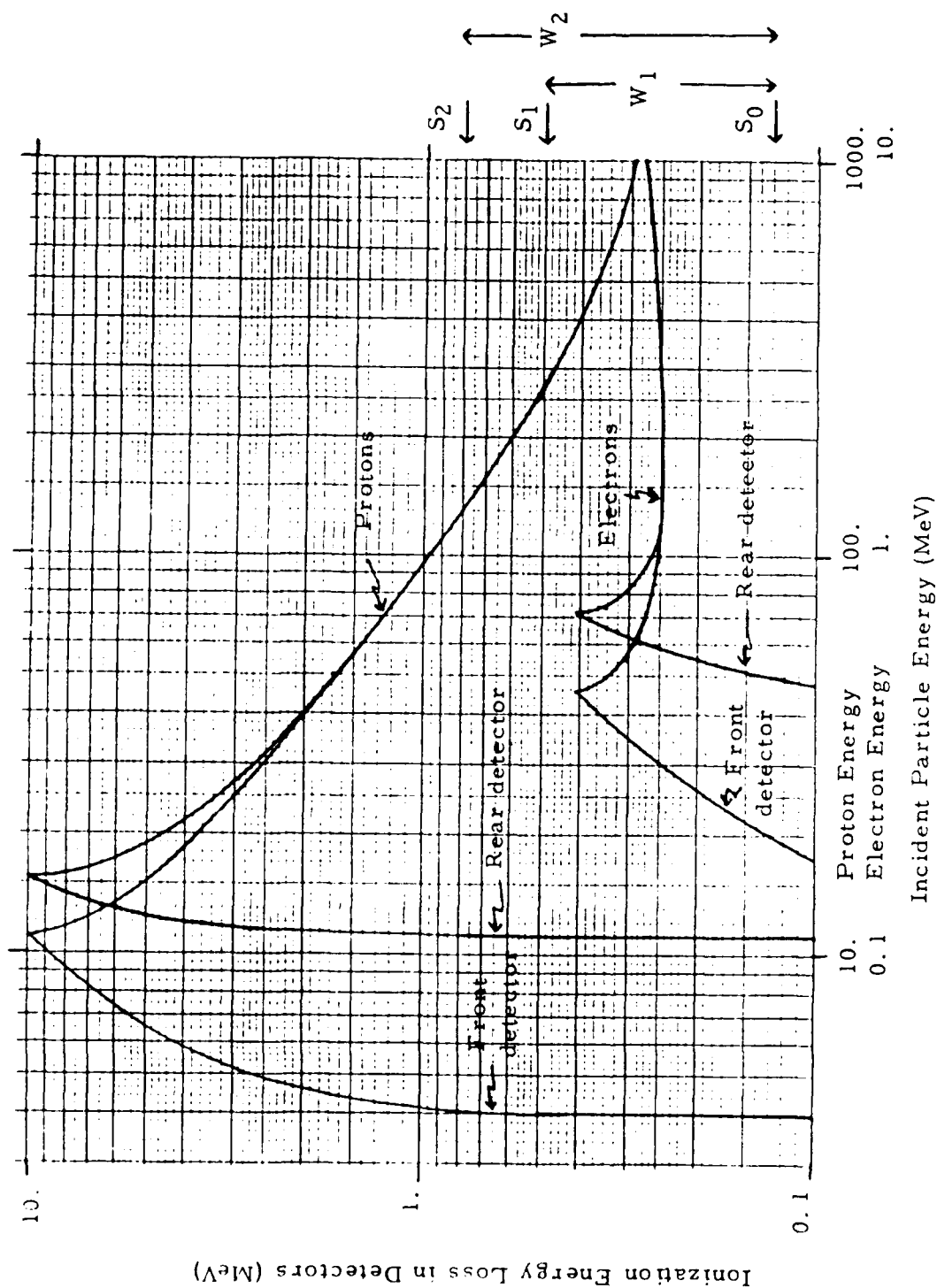
Figure 2.2   Ionization Energy Loss in the Silicon Solid State Detectors for Protons and Electrons.

5
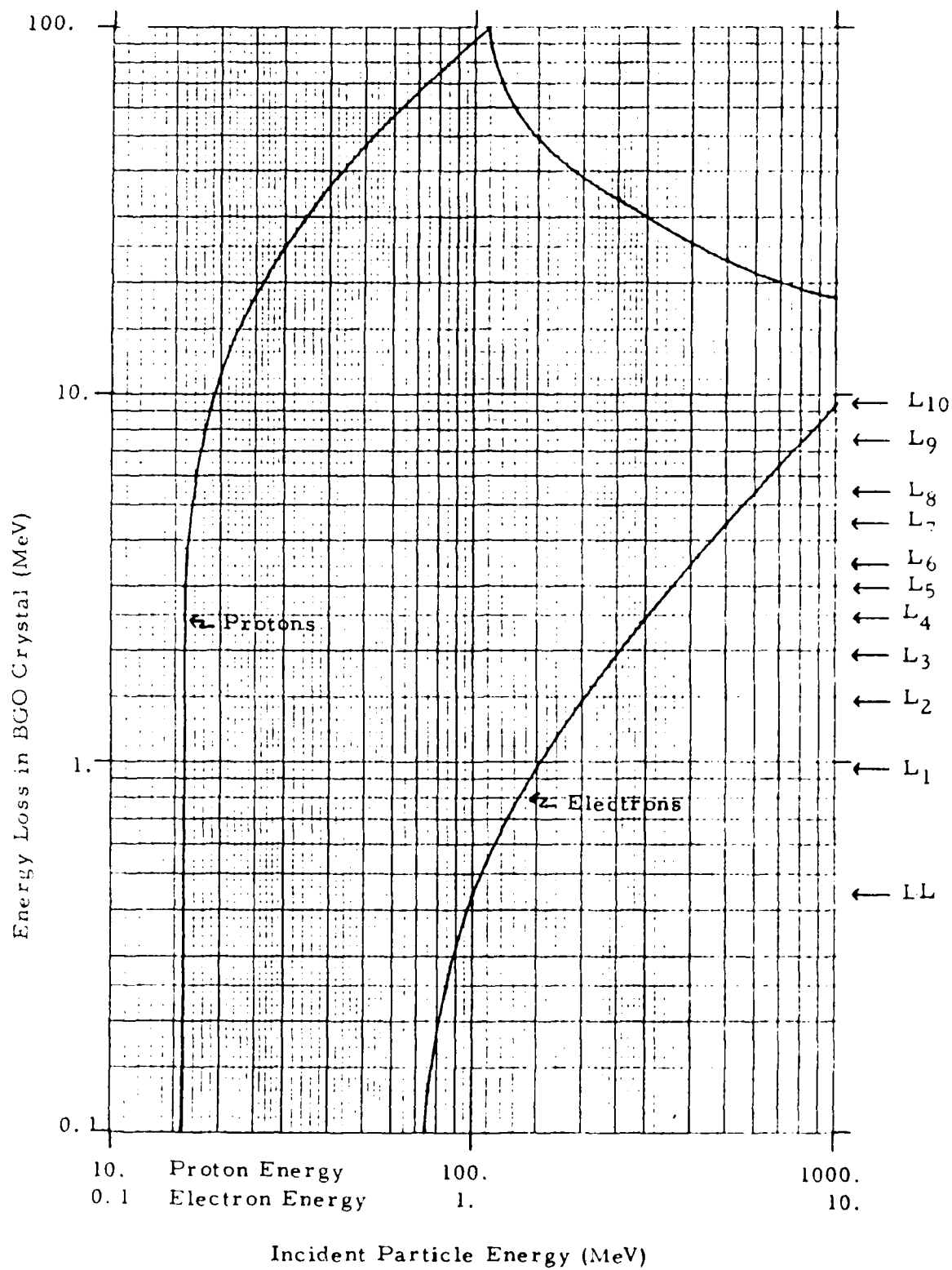
Figure 2. 3   Energy Deposited in the BGO Crystal by Protons
and Electrons

6

operation and correction of the electron data for accidental coincidences, should they be important. The telescope responses are based on the curves of Figs. 2.2 and 2.3, while the omnidirectional responses were obtained from similar calculations. The geometric factors are based on 100% particle detection, so electron scattering has been neglected. The energy ranges neglect the spread in particle energy loss, but this should not be a significant factor for the purpose of estimating channel count rates.

The response factors in Table 2.2 can be used with the estimated maximum particle fluxes in Tables 2.3 and 2.4 to obtain the maximum channel count rates with no coincidence requirements given in Table 2.5. The L = 1.6 electron and proton spectra have been used, except that the L = 4 AE 17 HI electron spectrum was used above 4 MeV. The count rates are rough calculations, since no detailed spectral interpolations were made, but should still be accurate to 20% if the input spectra are correct. Electron backscattering has been neglected except for the W_1, Front and W_2, Front total count rate, where it has been assumed that the Be foil will reduce the count rate to 1/3.

Table 2.1

Geometric Factor Information

A) Telescope View

Detector type	Defining Area (cm^2)	Half Cone Angle (deg)	Maximum Angle (deg)	Geometric Factor (cm^2-sr)
SSD, Front	0.732	15.6	24.3	0.167
SSD, Rear	0.219	7.5	10.6	0.0120
BGO				
Plastic	--	--	--	--

B) Omnidirectional Response

Detector type	Approximate W Shielding Equivalent (g/cm^2)	Approximate Geometric Factor (cm^2-sr)
SSD, Front	20	6.06
SSD, Rear	20	3.11
BGO	20	78.6
Plastic	15	525

7

Table 2.2

Channel Geometric Factors and Particle Detection Ranges

Channel Designation	Energy Loss (MeV)	Geometric Factors (cm²-sr)		Telescope Energy Ranges (MeV)		Omnidirectional Energy Ranges (MeV)
		Telescope	Omni	Electrons	Protons	Protons
Solid State Detectors						
> S_2, Front	> 0.80	0.167	6.06	-	4.2-130	116-265
> S_1, Front	> 0.50	0.167	6.06	-	4.1-269	116-588
W_1, Front	0.13-0.50	0.167	6.06	> 0.20	3.97-4.12/269-∞	115.51-115.65/588-∞
W_2, Front	0.13-0.80	0.167	6.06	> 0.20	3.97-4.24/130-∞	115.51-115.76/265-∞
> S_2, Back	> 0.80	0.0120	3.11	-	11.2-130	116-265
> S_1, Back	> 0.50	0.0120	3.11	-	11.1-270	116-588
W_1, Back	0.13-0.50	0.0120	3.11	> 0.52	11.00-11.13/270-∞	115.51-115.65/588-∞
W_2, Back	0.13-0.80	0.0120	3.11	> 0.52	11.00-11.23/130-∞	115.51-115.76/265-∞
BGO Crystal						
> $L_{10}s$	> 9.40	0.0120	78.6	> 10	19.3-∞	117-∞
> $L_{10}c$	> 9.40	0.0120	78.6	> 10	19.3-∞/(270-∞)	117-∞
L_9 - L_{10}	7.41-9.40	0.0120	78.6	8 - 10	18.5-19.3	116.29-116.51
L_8 - L_9	5.42-7.41	0.0120	78.6	6 - 8	17.7-18.5	116.07-116.29
L_7 - L_8	4.43-5.42	0.0120	78.6	5 - 6	17.3-17.7	115.96-116.07
L_6 - L_7	3.44-4.43	0.0120	78.6	4 - 5	16.9-17.3	115.84-115.96
L_5 - L_6	2.95-3.44	0.0120	78.6	3.5-4	16.7-16.9	115.79-115.84
L_4 - L_5	2.45-2.95	0.0120	78.6	3-3.5	16.5-16.7	115.73-115.79
L_3 - L_4	1.96-2.45	0.0120	78.6	2.5-3	16.3-16.5	115.68-115.73
L_2 - L_3	1.46-1.96	0.0120	78.6	2-2.5	16.1-16.3	115.62-115.68
L_1 - L_2	0.96-1.46	0.0120	78.6	1.5-2	15.9-16.1	115.57-115.62
LL - L_1	0.44-0.96	0.0120	78.6	1-1.5	15.7-15.9	115.51-115.57
Any BGO (> LL) > 0.44		0.0120	78.6	> 1	15.7-∞	116-∞
Plastic Shield Scintillator						
Ls	> 1.	-	625	-	-	48-∞

*For coincidence operation.

8

Table 2.3

Estimated Maximum Electron Fluxes for Design Purposes

Fluxes in electrons/(cm^2-sec-sr)

E	AE6-L-1.6		L=4				L=6.6			
			AE17 HI		AE17 LO		AE17 HI		AE17 LO	
(MeV)	Integral	Differential	Integral	Diff.	Integral	Diff.	Integral	Diff.	Integral	Diff.
0.2	1.7+7	1.4+7	1.2+6	4.0+5	1.2+6	4.0+5	4.8+5	2.6+5	4.8+5	2.6+5
0.5	2.5+6	1.9+6	8.0+5	5.5+5	8.0+5	5.5+5	2.2+5	1.5+5	2.2+5	1.5+5
1.0	6.8+5	2.8+5	2.5+5	1.3+5	2.5+5	1.3+5	6.7+4	5.1+4	6.7+4	5.1+4
1.5	4.0+5	1.3+5	1.2+5	4.0+4	1.2+5	5.6+4	1.6+4	1.2+4	1.6+4	1.2+4
2.0	2.7+5	7.3+4	8.0+4	1.6+4	6.4+4	2.5+4	4.0+3	2.8+3	4.0+3	2.8+3
2.5	2.0+5	4.5+4	6.4+4	8.0+3	3.9+4	1.9+4	1.2+3	8.8+2	1.2+3	8.8+2
3.0	~1.5+5	~3.0+4	5.6+4	8.0+3	2.0+4	1.2+4	3.2+2	1.7+2	3.2+2	1.7+2
3.5	~1.2+5	~2.1+4	4.8+4	1.0+4	8.0+3	4.8+3	1.5+2	7.0+1	1.5+2	7.0+1
4.0	~1.0+5	~2.8+4	3.8+4	3.0+4	3.2+3	3.0+3	8.0+1	6.0+1	8.0+1	7.8+1
5.0	~7.5+4	-	8.0+3	7.4+3	1.6+2	1.6+2	2.0+1	1.9+1	2.0+0	-
6.0	-	-	6.4+2	6.3+2	1.4+0	-	1.0+0	-	-	-
8.0	-	-	~1.2+1	~1.1+1	-	-	-	-	-	-
10.0	-	-	~0.8+0	-	-	-	-	-	-	-

Note: (1) $N + m = N \times 10^m$

(2) Integral fluxes are for $\geq$ E; Differential fluxes are for that energy to the next table energy.

(3) The approximate sign (~) is used for fluxes extrapolated from the various sources.

9

Table 2.4 Estimated Integral Proton Fluxes
Integral Flux [p/cm^2-sec)]

E	L=1.6 ($B=B_0$)	L≥4
MeV	AP8 MAX	Cosmic Rays
4	4.0+5	3.23
8	2.7+5	3.23
10	2.0+5	3.23
20	6.5+4	3.23
40	3.0+4	3.25
60	2.1+4	3.21
80	1.7+4	3.21
100	1.4+4	3.1S
150	7.6+3	3.13
200	4.3+3	3.07
250	2.4+3	2.99
300	1.6+3	2.90
350	8.5+2	2.81
400	5.8+2	2.70

Notes: (1) Read N+n as $Nx10^{\pm n}$
(2) AP8 MAX shows no protons above
8 MeV for L≥4 at $B=B_0$.
(3) 4πsr isotropy assumed in cosmic
ray primaries.

10

Table 2.5

Estimated Maximum Channel Count Rates

Channel Designation	Maximum estimated count rate (cps) for			
	Telescope		Omnidirectional	
	Electron	Proton	Proton	Total
$> S_2$, Front	-	$5.3 + 3$	$5.8 + 3$	$1.1 + 4$
$> S_1$, Front	-	$5.3 + 3$	$5.8 + 3$	$1.1 + 4$
W_1, Front	$2.9 + 6$	$7.0 + 1/3.2 + 1$	$1.4 + 0/2.8 + 2$	$(= 1 + 6)$
W_2, Front	$2.9 + 6$	$1.3 + 2/1.4 + 2$	$1.5 + 1/1.2 + 3$	$(= 1 + 6)$
$> S_2$, Back	-	$1.6 + 2$	$3.0 + 3$	$3.2 + 3$
$> S_1$, Back	-	$1.7 + 2$	$3.0 + 3$	$3.2 + 3$
W_1, Back	$3.1 + 4$	$1.4 + 1/1.9 + 0$	$4.4 + 0/1.4 + 2$	$3.1 + 4$
W_2, Back	$3.1 + 4$	$1.6 + 1/1.0 + 1$	$7.9 + 0/5.9 + 2$	$3.1 + 4$
$> L_{10\,s}$	$9.5 - 3$	$6.2 + 1$	$7.6 + 4$	$7.6 + 4$
$> L_{10\,C}$	$9.5 - 3$	$6.2 + 1/2.0 + 0$	$7.6 + 4$	$7.6 + 4$
$L_9 - L_{10}$	$1.3 - 1$	$1.0 + 1$	$1.8 + 2$	$1.9 + 2$
$L_8 - L_9$	$7.1 + 0$	$1.0 + 1$	$1.8 + 2$	$2.0 + 2$
$L_7 - L_8$	$8.7 + 1$	$5.1 + 0$	$8.8 + 1$	$1.8 + 2$
$L_6 - L_7$	$3.6 + 2$	$5.0 + 0$	$9.6 + 1$	$4.6 + 2$
$L_5 - L_6$	$3.4 + 2$	$2.5 + 0$	$4.0 + 1$	$3.8 + 2$
$L_4 - L_5$	$4.5 + 2$	$2.5 + 0$	$4.8 + 1$	$5.0 + 2$
$L_3 - L_4$	$6.3 + 2$	$2.5 + 0$	$4.0 + 1$	$6.7 + 2$
$L_2 - L_3$	$9.5 + 2$	$2.5 + 0$	$4.8 + 1$	$1.0 + 3$
$L_1 - L_2$	$1.6 + 3$	$2.5 + 0$	$4.0 + 1$	$1.7 + 3$
$LL - L_1$	$3.5 + 3$	$2.5 + 0$	$4.8 + 1$	$3.5 + 3$
Any BGO($> LL$)	$7.4 + 3$	$1.3 + 2$	$7.6 + 4$	$8.4 + 4$
LS	-	-	$5.8 + 5$	$5.8 + 5$

Notes: (1) $N + n \equiv N \times 10^n$

(2) Electron spectrum is $L = 1.6$ to 4 MeV, $L = 4$ AEI7 HI for > 4 MeV.

(3) Proton spectrum is $L = 1.6$

(4) Electron count rates neglect backscattering, except the W_1, Front and W_2, Front totals where about $1/3$ transmission by the Be foil is assumed.

(5) No coincidence requirements

(6) $> L_{10\,s}$ is a singles channel; $> L_{10\,C}$ is a coincidence channel, with the second telescope proton count rate being for the coincidence mode.

11

2.3 Coincidence Resolving Time Effects

Under normal operation the electron measurements require a triple coincidence between the two SSD's and the BGO crystal, and an anticoincidence with the plastic shield scintillator. As described in more detail in section 3, the fast timing coincidence is done with 65 nsec wide pulses, and a minimum overlap of 15 nsec is required to trigger the logic. These properties of the coincidence circuitry allow the accidental count rates to be calculated for high input count rates.

For two pulses of width T and a required minimum overlap of the circuit resolving time is given by

$$\tau = 2(T - \Delta) \tag{2.1}$$

which gives τ = 100 nsec for T = 65 nsec and Δ = 15 nsec. The output pulses from a dual pulse coincidence will have a uniform distribution from 0 to T in width, with only pulses wider than Δ being usable. The average usable pulse width is $(T + \Delta)/2$ = 40 nsec. The third pulse coincidence thus has an average resolving time of

$$\tau_3 = T + (T + \Delta)/2 - 2\Delta = 75 \text{ nsec}, \tag{2.2}$$

and for input count rates N_1, N_2 and N_3, the accidental coincidence count rate is

$$N_{acc} = N_1 N_2 N_3 \, \tau \tau_3 . \tag{2.3}$$

For the estimated maximum count rates of Table 2.5 we have N_1 (W_1 or W_2, front) ~ 1 x 10^6/sec, N_2 (W_1 or W_2, back) ~ 3.1 x 10^4/sec so

$$N_{acc} \text{ (BGO)} = 2.3 \times 10^{-4} \, N_i \text{ (BGO)} \tag{2.4}$$

where N_i (BGO) is the singles count rate of the BGO crystal in pulse height channel i. The results of using (2.4) with the BGO total count rates of Table 2.5 are given in Table 2.6. For the electron/proton spectra used for Table 2.5, the triple coincidence rate is much lower than the true electron count rate, except for the very highest channels (L_9 - L_{10}, and > L10c).

Table 2.6

Accidental Coincidence Count Rates

Channel Designation	True Coincidence Count Rate (cps)	Accidental Triple Coincidences		Accidental Double Coincidences	
		Count Rate (cps)	Acc/True	Count Rate (cps)	Acc/True
$> L_{10}$ s	(7.6 + 4)	1.8 + 1	2.6 + 0	2.4 + 2	3.4 + 1
$> L_{10}$ c	2.0 + 0	1.8 + 1	1.9 + 3	2.4 + 2	2.5 + 4
$L_9 - L_{10}$	1.3 - 1	4.4 - 2	3.4 - 1	5.9 - 1	4.5 + 0
$L_8 - L_9$	7.1 + 0	4.7 - 2	6.6 - 3	6.2 - 1	8.7 - 2
$L_7 - L_8$	8.7 + 1	4.2 - 2	4.8 - 4	5.6 - 1	6.4 - 2
$L_6 - L_7$	3.6 + 2	1.1 - 1	3.1 - 4	1.4 + 0	3.9 - 3
$L_5 - L_6$	3.4 + 2	8.8 - 2	2.6 - 4	1.2 + 0	3.5 - 3
$L_4 - L_5$	4.5 + 2	1.2 - 1	2.7 - 4	1.6 + 0	3.6 - 3
$L_3 - L_4$	6.3 + 2	1.6 - 1	2.5 - 4	2.1 + 0	3.3 - 3
$L_2 - L_3$	9.5 + 2	2.3 - 1	2.4 - 4	3.1 + 0	3.3 - 3
$L_1 - L_2$	1.6 + 3	4.0 - 1	2.5 - 4	5.3 + 0	3.3 - 3
$LL - L_1$	3.5 + 3	8.1 - 1	2.3 - 4	1.1 + 1	3.1 - 3

Notes: (1) $N + n \equiv N \times 10^n$

(2) Double Coincidences are SSD (back) + BGO

(3) All true coincidences are electrons (except $> L_{10}$ which is a singles channel), and no efficiency reductions for scattering effects are included.

13

For reference, the double coincidence accidentals count rate is also given, for the SSD (back) + BGO set, $(N_{acc} = N_2 N_3 \tau)$, ,and is seen to provide a poorer result than the triple coincidence by about a factor of 10.

The highest expected count rates in Table 2.5 should not cause any problems. The SSD's and the plastic scintillator pulses are shaped so that most of the pulse (double peaked) is over in about 1.5 microsec. For these the problem of pileup will only become significant at count rates above a few hundred kHz. The front SSD will have some pileup if the count rate does go to 1×10^6/sec, but this would be only for the worst case L = 1.6 electron spectrum. The BGO crystal pulse is shaped to be over in about 3 microsec, so it can operate to about 100 kHz with no pileup. Thus, all detectors should not have pileup problems, with the possible exception of the front SSD at L = 1.6.

The plastic anticoincidence shield has a maximum expected count rate of about 5.8×10^5/sec (Table 2.5), from high energy penetrating protons. For a completely random time distribution it can be shown that the triple coincidence pulses have an average width of

$$\overline{T}_3 = \frac{T + (T - 3\Delta)\ (5/2 - 4\ln 2)}{8\ln 2 - 4} \tag{2.5}$$

where T = 65 nsec is the input pulse widths, assumed equal for all three input pulses, and Δ = 15 nsec is the minimum required output pulse width. The result is T_3 = 38.5 nsec, and this gives a dead time from the plastic scintillator as

$$T_d = T + 2\Delta - \overline{T}_3$$

$$= 56.6 \text{ nsec} \tag{2.6}$$

At the maximum count rate this gives a plastic scintillator caused dead time fraction of $56.5 \times 10^{-9} \times 5.8 \times 10^5$ = .033, for a 3.3% data loss. The true data triple coincidence come from time correlated rather than random pulses, so the value of T_3 for true data may be slightly different from (2.5). However, since the coincidence circuit input pulse widths are set to the narrowest possible without significant loss of data from the intrinsic time jitter in the pulses, the result (2.5) is likely to be a good approximation. Thus, dead time corrections to the data are not expected to be significant, with the maximum being about 3%.

3.0 DETAIL DESIGN

3.1 System

The High Energy Electron Analyzer (also referred to as Fluxmeter) consists of 2 subassemblies: the Sensor subassembly and the Data Processor Unit (DPU) subassembly. The two subassemblies are connected together with an approximately 1 ft shielded cable. The Sensor electronics includes four preamplifiers (one for each detector) and the H.V. supply for the 3 photomultipliers (PMT's). The DPU contains all other electronics.

The High Energy Electron Analyzer can best be described with the aid of the block diagram of Fig. 3.1. In-aperture electrons in the range 1-10 MeV deposit sufficient energy in each of the three detectors (front and back solid state detectors and BGO crystal), configured in a properly defined telescope arrangement, such that the signals derived from them will satisfy a triple coincidence requirement. This requirement guarantees a high level of rejection of accidental coincidence possibilities and provides needed protection against "corner-cutting" protons. The output signal of a fourth detector (plastic scintillator surrounding the BGO crystal) serves as an additional guard against accidental coincidences due to corner-cutters and omnidirectional protons, by negating the triple coincidence.

The four detectors thus possess the following veto characteristics against cosmic ray and other high energy protons:

1) Very large entrance angle protons cannot produce a coincidence in the Solid State detectors. Additionally, those which do pass through the back Solid State detector and deposit an energy < 10 MeV in the BGO will be vetoed by the plastic shield even if an <u>accidental</u> coincidence is produced by spurious radiation in the front Solid State detector.

2) The extreme entrance angle protons that can produce a Solid State detector coincidence will be vetoed either by the shield or by > 10 MeV energy loss in the BGO.

3) The small angle, in-aperture, protons > 130 MeV, which make the proper Solid State detector coincidence but do not intercept the shield will be vetoed by > 10 MeV energy loss in the BGO.

For the lower energy in-aperture protons, < 130 MeV, no coincidence is produced by the solid state detectors and therefore they are vetoed. In the following, reference is made to the energy deposition diagrams in Section 2.1 for p's and e's in the solid state detectors (SSDs) and the scintillation crystal (BGO).

15

The diagrams indicate the deposited energy levels (L) in the BGO, and the deposited energy levels (S) and windows (W) in the SSDs.

Each electron of proper energy (1-10 MeV) which enters the aperture will create photons in the scintillation crystal and a charge pulse in each SSD. The photons produced in the crystal are optically coupled to the photocathode of photomultiplier A (PMT-A). The resulting charge pulses at the anode are processed by the CSPA-shaping amplifier-voltage amplifier chain, and passed along to the BGO Pulse Height Analyzer (PHA) via the zero crossing detector/single channel analyzer (ZCD/SCA). The latter produces a very fast output pulse (BGO COINC) for any electron of incident energy > 1 MeV.

Two identical Charge Sensitive Preamplifiers (CSPA) and associated Pulse Height Analyzers (PHA) process the charge pulses from the front and back solid state (semiconductor) detectors (SSD), respectively. This processing results in a rough energy distribution determined by windows W_1 and W_2 and by 2 thresholds S_1 and S_2. In addition, the two windows (W_1 and W_2), set in each PHA, are put into fast coincidence with the BGO COINC. signal to identify positively that an electron entering from the front of the detectors (see arrow) is to be analyzed. Analysis of the BGO PULSE, SHAPED is then carried out in the BGO Pulse Height Analyzer for 10 differential energy ranges and 2 energy threshold ranges. Energetic Protons which create photons in the anticoincidence shield are detected by PMT-B and PMT-C, the anode pulses of which are summed and processed by a CSPA-shaping amplifier-voltage amplifier chain. Again a ZCD/SCA produces a very fast timing pulse (SHIELD COINC.) which is used to veto triple coincidences as described above. The uniform output pulses from the SSD and BGO PHAs plus one additional output from each ZCD/SCA labeled ANY BGO PULSE and ANY SHIELD PULSE are accumulated in an array of 22 compression counters. The contents of these counters are parallel-transferred to shift registers where they are serially read out by the spacecraft data processing system every ˜1/2 second. The read rate is 264 bits/readout, which is 528 bits/sec.

The fast timing pulses from the W output of the SSDs and the SHIELD COINC. are delayed to accommodate the slower decay time of the BGO crystal. Thus, a fast triple coincidence (BGO COINC., W front and W back) or veto (SHIELD COINC.) is assured by the 4-input AND gates (coincidence gates). The coincidence requirement of the front (CRF) and back (CRB) SSD's as well as the anti-coincidence requirement (ACR) of the plastic shield are enabled or disabled individually on ground command.

This makes it possible to verify proper operation of the individual detectors and their electronics by means of the calibration source, and by changes in the channel count rates from the ambient fluxes.
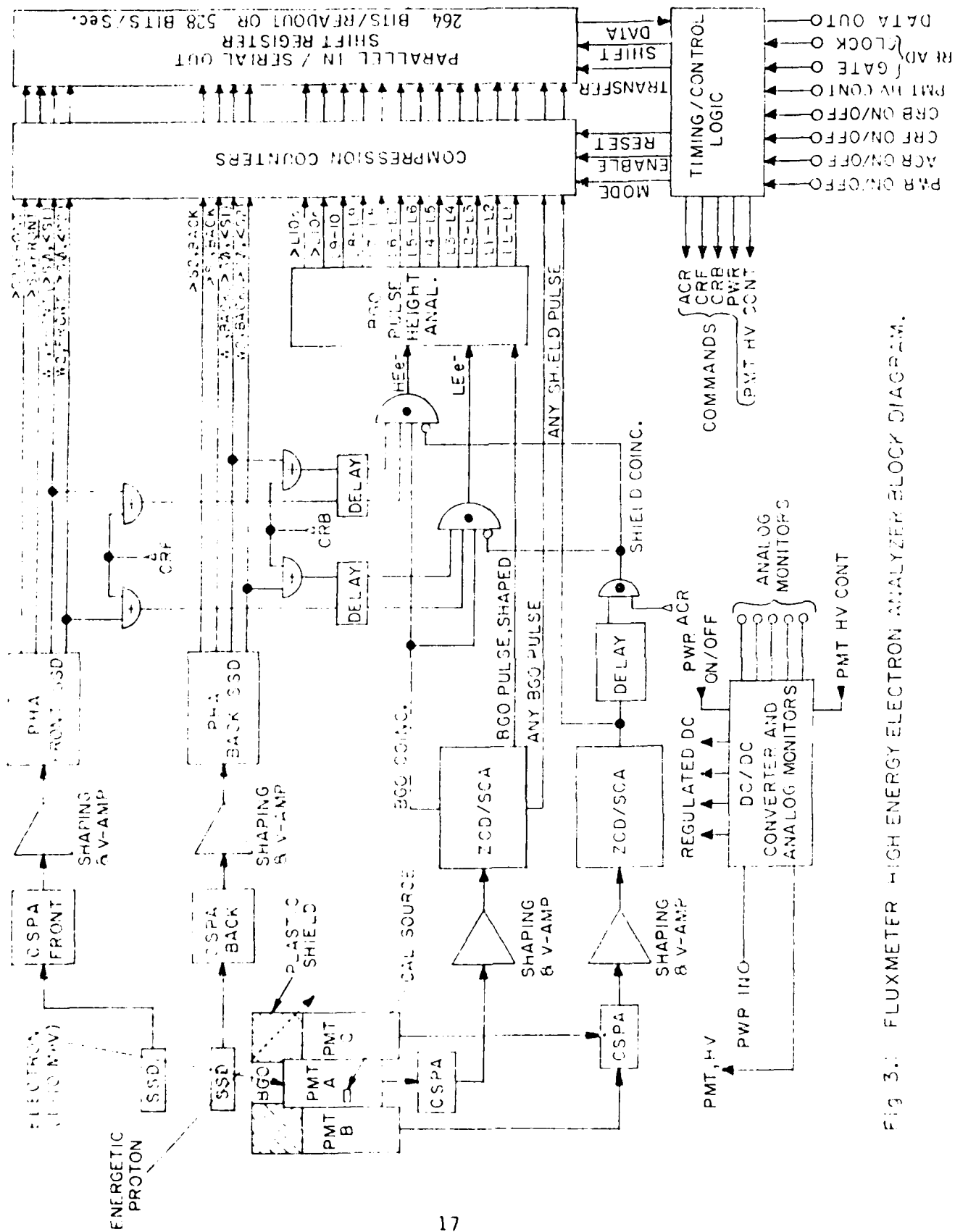
Fig 3. FLUXMETER HIGH ENERGY ELECTRON ANALYZER BLOCK DIAGRAM.

17

The calibration source is a 10 nCi source, mounted towards the rear of the Sensor. The source produces a peak at 1.25 MeV in the BGO crystal, and is therefore centered in the L_1-L_2 channel. This is ideal for checking the gain of the BGO PMT. It should be noted that the BGO PMT gain measurement with the Co-60 source can only be made in the absence of significant ambient fluxes above the cosmic ray background.

All signals to and from the spacecraft are interfaced with the instrument through the Timing/Control Logic. Low voltage power is derived from the 28V spacecraft bus via a DC/DC converter, which also supplies analog monitors of the secondary output voltages and a bi-level power ON/OFF monitor.

The PMT HV and the SSD bias voltages are derived from the +12V output of the DC/DC converter via pulse width modulated power supplies. The PMT HV output is adjustable by ground command. Analog monitors of the PMT HV and the SSD bias voltage are available at the telemetry interface connector. The DPU and Sensor temperatures are continuously monitored with positive temperature coefficient thermistors. Both monitors are available for telemetry.

3.2 BGO and Shield Pulse Processing Circuits

A block diagram of the BGO Pulse Processing Circuit is shown in Figure 3.2, top. The charge pulses from the BGO photomultiplier anode are converted to voltage pulses by a charge sensitive preamplifier located in the sensor assembly. These pulses are then integrated, differentiated and amplified by the shaping and voltage amplifier. The time constants used in the shaping amplifier are of the order of .3 μs, matching the crystal decay constant of the BGO crystal. The conversion gain of the preamplifier-shaping and voltage amplifier combination are set during initial calibration to about .35 V/MeV. The shaped pulses (BGO PULSE, SHAPED) are directly applied to the BGO PHA. Two more outputs are derived from this processing circuit: BGO COINC. and the ANY BGO PULSE outputs.

The latter is the stretched pulse output from the zero crossing detector (ZCD), timed by the fast single shot multivibrator (Fast O/S.) This pulse represents the presence of any e^- or p^+ (without coincidence requirement) which deposits an energy above the LL threshold set in the single channel analyzer (SCA). This threshold is set to 0.44 MeV representing the lowest threshold of the BGO-PHA. Output pulses derived in this manner are directly accumulated in one of the compression counters.

A second pulse, BGO COINC., is also derived from the ZCD and fast O/S, providing the input for the fast coincidence circuits, HE_e and LE_e. The ZCD provides stable timing of the coincidence output because the zero crossing of the shaped amplifier pulse is largely independent of pulse height. The fast O/S determines a stable, short pulse width of about 65 ns. The stability and shortness of these pulses are of importance for the fast triple

18

coincidence with the front and back SSD timing pulses (W). A more detailed description of the triple coincidence gates is given in Section 3.

The Shield Pulse Processing Circuit is shown in Fig. 3.2, bottom. As described in detail at the beginning of this section, the shield serves as a guard against energetic protons. They are detected by the plastic scintillator/PMT B and C combination. The charge output of the 2 PMTs is summed in a charge sensitive preamplifier (located in the Sensor) in order to obtain output pulses of nearly equal amplitude from protons regardless of their point of incidence on the shield. After summing, the pulses are applied to a shaping and voltage amplifier with time constants matching the extremely fast decay constants of the plastic. Processing of the shaped pulses is similar to that described above, except that the SCA disables the ZCD for all protons below approximately 1 MeV energy deposited in the shield. Thus, all energy deposits above 1 MeV will produce a SHIELD COINC. pulse. This operation provides a veto at the triple coincidence gate for accidental triple coincidence possibilities. Because of the short amplifier time constants the veto pulse must be delayed in order to arrive simultaneously at the coincidence gate with the slower BGO and SSD timing pulses. This is accomplished with a mono-stable delay circuit. Again, the ZCD and the fast O/S provide a stable 65 ns timing pulse at the shield coincidence output. A second output, ANY SHIELD PULSE is derived from the ZCD prior to the delay circuit. As the name implies, any shield pulse (above ≊1 MeV) is output and connected to a compression counter after pulse stretching.

3.3 SSD Pulse Shaping Circuits

High energy electrons entering the aperture pass through 2 solid state detectors (SSD). Both are totally depleted silicon surface barrier diodes with a depletion depth of 700 micron and an active area of 100 mm^2 for the front and 50 mm^2 for the back detector. The energy deposited in each detector for incident electrons of range 1-10 MeV is shown in the energy deposition diagrams of Section 2.1.

The deposited energy in each detector produces a charge pulse, proportional to that energy, at the output of the detector. Unlike the PMTs used for the BGO and Shield proton detection, the SSds have no intrinsic gain. For this reason preamplifiers of special, low noise design must be employed for amplification. These are the charge sensitive preamplifiers (CSPA) shown in Fig, 3.1. These are hybrid microcircuits manufactured by Amptek and available screened to MIL 883B. The input stage of these devices is configured as a charge sensitive preamplifier while the second stage provides a double integration and differentiation. Thus, the output is a bipolar pulse with a shaping time constant of nominally 250 ns. The input equivalent noise of this preamplifier/shaping amplifier combination is specified as 15 keV
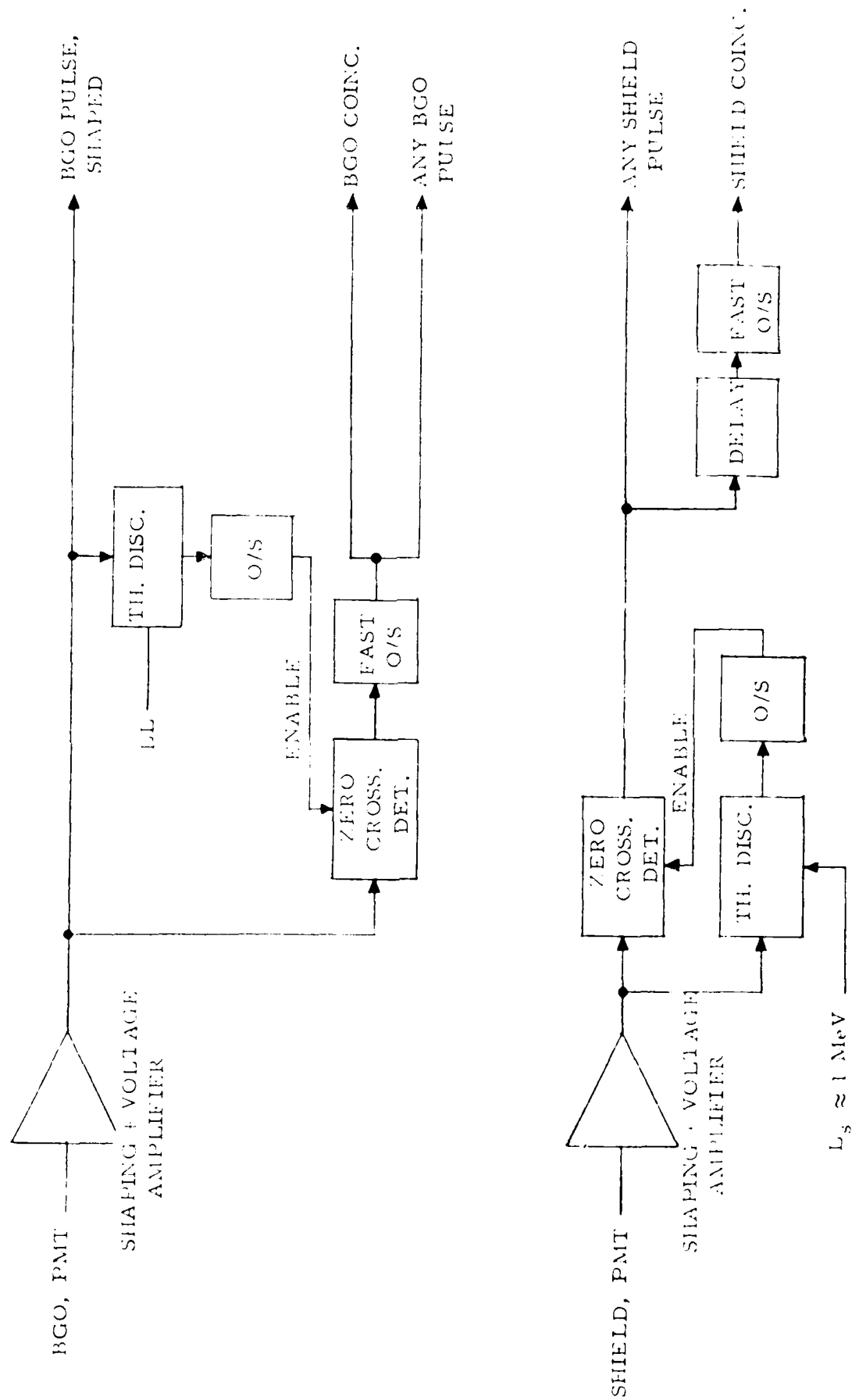
Fig. 3.2 BGO AND SHIELD PULSE PROCESSING CIRCUIT WITH FAST TIMING OUTPUTS.

FWHM (Si). The noise contribution from the following voltage amplifier is negligible. The detector noise (beta resolution) of a 100 mm^2, 700 micron thick Ortec surface barrier detector is given as 10 keV FWHM. It is slightly less for a 50 mm^2 detector of the same thickness. Thus the SSD system noise is estimated as

$$\Delta E = \sqrt{15^2 + 10^2} = 18 \text{ keV FWHM (Si)}$$

Since a threshold may be set to 2.5 times this value for less than 1 noise count per second, it would be possible to set it as low as 45 keV. This is about a factor of three below the lowest threshold (S_O) to be set and will present no problem for a five-year life span. The overall conversion gain of the CSPA-Shaping-Voltage amplifier combination is set during initial calibration to approximately 1V/MeV.

An important feature of the CSPA is the immunity of its conversion gain to changes in detector and stray capacitance. This immunity is further enhanced by placing the CSPA as close to the detectors as possible, namely at the rear of the sensor subassembly.

3.4 SSD Pulse Height Analyzer

The analog pulse outputs from the SSD shaping amplifiers are analyzed by two identical pulse height analyzers (PHA); one for each SSD. Fig. 3.3 shows one of the 2 PHAs in diagrammatic form. Three identical threshold discriminators and a ZCD interrogate the CSPA/Amp. output pulse simultaneously. The discriminators produce an output pulse any time their particular threshold (S$\emptyset$, S1 or S2) is exceeded. The thresholds are set by a voltage divider string connected to a stable voltage reference. The ZCD which is enabled only when the lowest threshold (S$\emptyset$) is exceeded, triggers a fast O/S when the amplifier pulse crosses its zero volt base line. Because the zero crossing occurs always after a discriminator pulse has terminated, the latter is stretched with a O/S to overlap the fast O/S pulse width. Strobing the higher level (S1 and S2) discriminator outputs with the fast O/S pulse (≂65 ns pulse width) at the inputs of the AND gates defines 2 energy windows (> S$\emptyset$, < S1 and > S$\emptyset$, < S2). Thus, depending on the pulse height of the amplifier signal a logic pulse W1 or W2 is strobed out. Either pulse is referenced in time to the stable zero crossing of the amplifier signal and has a stable pulse width of ≂65 ns determined by the strobe pulse. In addition to the window signals (differential energy) the logic pulses > S1 and > S2 are available at the output. They represent an electron or proton which has exceeded a certain energy threshold, the equivalent of which is set by the respective threshold voltage S1 and S2. The 4 logic outputs from each SSD are counted in four individual compression counters.
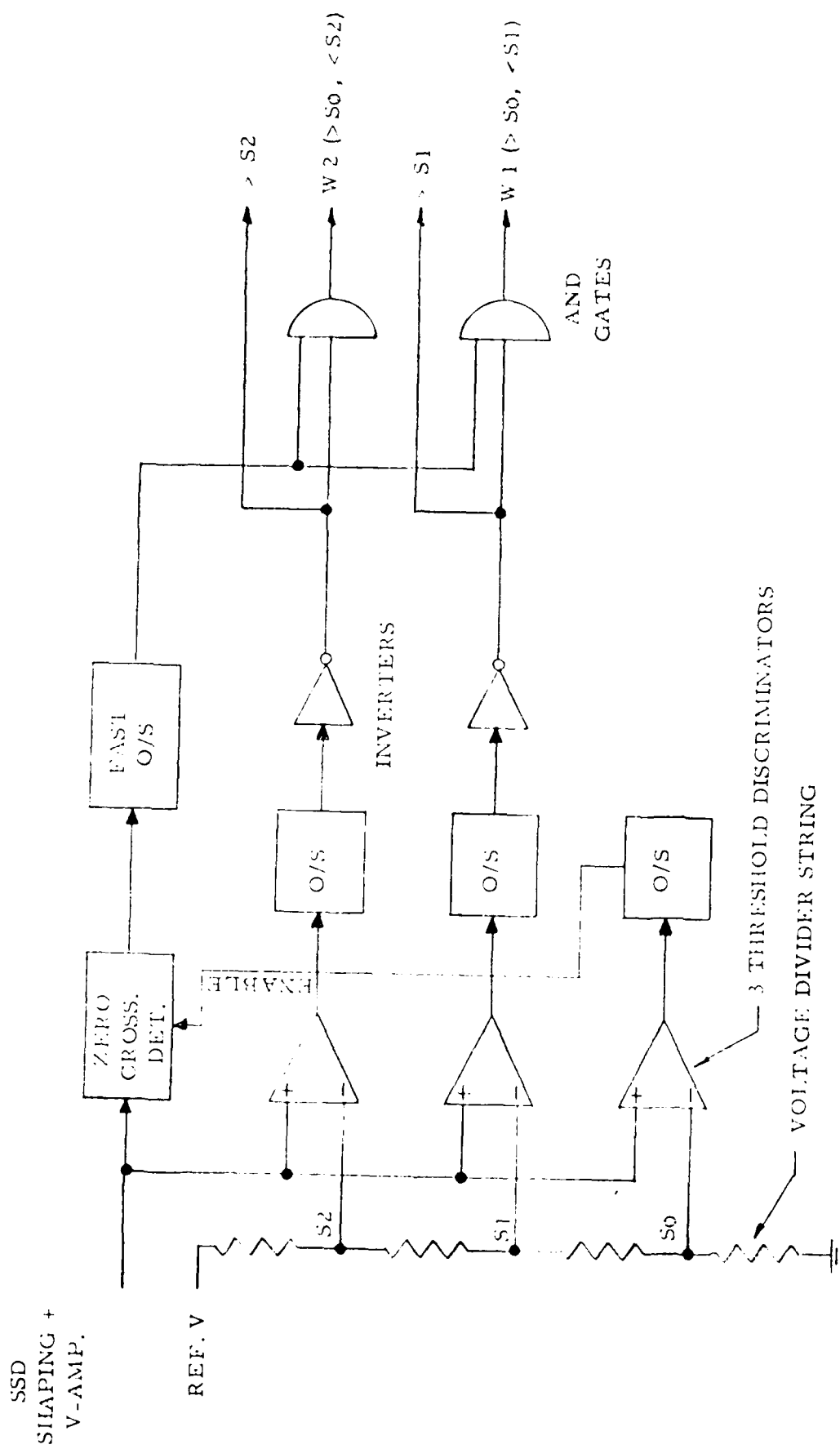
> S2

W 2 (> So, < S2)

> S1

W 1 (> So, < S1)

AND
GATES

INVERTERS

FAST
O/S

ZERO
CROSS.
DET.

O/S

O/S

O/S

ENABLE

3 THRESHOLD DISCRIMINATORS

VOLTAGE DIVIDER STRING

+

−

+

−

+

−

S2

S1

So

SSD
SHAPING +
V-AMP.

REF. V

Fig. 3.3 SOLID STATE DETECTOR - PULSE HEIGHT ANALYZER

(One of two shown)

22

The main purpose of the W1 and W2 outputs, however, is to establish a fast triple coincidence with the BGO pulses. This requirement and its implementation is discussed in the following section.

3.5 Fast Triple Coincidence Gates

Two identical triple coincidence gates are used: one for high energy electrons (HEe-) and one for low energy electrons (LEe-) as shown in Fig. 3.1. Either gate creates a logic output whenever the timing signals from the front (W front) and back (W back) SSDs coincide with a timing signal from the crystal (BGO COINC.) Each of the 3 timing signals is referenced to the zero crossing of their respective shaped pulse outputs from the 3 detectors. Since the shaped pulse from the BGO is the slowest (dictated by its .3 us crystal decay time) the start of the timing signals from the other two detectors (SSD) must be delayed, such that the coincidence is established at the gate inputs. This is indicated in Fig. 3.1 by the 2 delay circuits in the W1 and W2 signal lines. As mentioned in previous sections, the timing signals must be stable and of very short duration to reduce random or chance coincidences. This is supported by the well known expression for a 2 input coincidence gate:

$$N_r = 2 C_1 C_2 \tau \qquad\qquad (3.1)$$

where N_r = rate of random coincidences, C_1, C_2 = average rate of input pulses and τ = coincidence gate resolving time. It can be seen that τ must be as small as possible to reduce N_r especially at high counting rates C_1 and C_2, which are expected for this application. The gate resolving time can be expressed as [see Equation (2.1) also]:

$$\tau = 2 (T - \Delta) \qquad\qquad (3.2)$$

where T = timing signal pulse width, Δ = minimum time for gate to respond. From equation (3.2) it is obvious that T must be as small as practical. The minimum practical pulse width is about 65 ns. The coincidence gate itself is a low power Schottky device with a typical response time of 15 ns. Substituting these values in Equation (3.2) gives a coincidence resolving time of approximately 100 ns.

The above evaluation of Equations (3.1) and (3.2) is for a 2 input coincidence gate. For a three-input gate the analysis has been given in Section 2.1.3, along with estimates of the effects at the highest expected count rates. The fourth input derived from the plastic shield is used in anti-coincidence with the 3 timing signals from the electron detecting telescope (BGO and 2 SSDs). Because of the very fast plastic decay time (order of 10^{-8}s) the shaping time constants for that pulse shaping amplifier

23

are small compared to the BGO pulse amplifier. Therefore, the zero crossing time for plastic shield pulses is small compared to that of BGO pulses, and a delay must be introduced for anticoincidence pulses produced by the shield. This is depicted in Fig. 3.1. For the same reason as stated above, namely to reduce the error from random anticoincidence pulses, the pulse width of the shield pulse is made as short as practical. It is 65 ns.

To summarize, the timing signals (coincidence and anticoincidence pulses) are referenced to the zero crossovers of the shaped pulses from the 4 detectors to minimize time jitter. A time delay is introduced after the crossover for the SSD and shield pulses to achieve coincidence with the slower BGO pulses. Fast, stable O/S's are triggered by the leading edge of the zero crossover (BGO signal) and the leading edge of the delayed crossover (SSD and shield signal), resulting in timing pulses of 65 ns width. Finally, these timing pulses are applied to an AND gate (coincidence gate) to detect the coincidence in the BGO and SSD's of in-aperture electrons or to veto (shield pulse) such a coincidence due to a proton or false coincidence. The two pulse coincidence resolving time is approximately 100 ns.

Two identical coincidence gates are used to reduce the possibility of high energy proton contaminates of the high energy electron channels. The gate for the high energy electrons (HEe-) is connected to the W1 outputs of the front and back SSD-PHAs while the gate for the low energy electrons (LEe-) is connected to the W2 outputs of the same PHAs.

3.6 BGO Pulse Height Analyzer

A detailed block diagram of the BGO-PHA is shown in Fig. 3.4. The shaped pulses from the BGO pulse amplifier are applied simultaneously to 10 comparator/OS's. The comparator threshold levels (L1 through L10) are fixed by a voltage divider string supplied with a stable reference voltage. A O/S output occurs from any Comparator/OS which detects a pulse amplitude larger than its respective threshold (L1 and L10). Combining 2 such outputs from 2 successive comparators in a logic AND gate defines a pulse amplitude window or a differential energy bin due to the proportionality of pulse amplitude vs. deposited energy. Ten comparators with thresholds L1 through L10 are combined in this manner to yield 9 energy bins L1-L2, L2-L3 ... and L9-L10. The lowest energy bin (LL-L1) is obtained simply by putting the comparator L1 output into anticoincidence with the coincidence output LEe- which is only present if the LL thresholds set in the BGO zero cross detector is exceeded. The AND gates are strobed by the coincidence gate outputs mentioned in the previous section. The 3 lowest energy logic gates are strobed by the low electron energy coincidence pulses (LEe-) and the remaining 7 gates are strobed by the high electron energy coincidence pulses (HEe-). Thus, an output pulse at one of the gates LL-L1, L1-L2, etc. represents an electron of a certain differential energy which has passed through the 2 SSDs and the BGO crystal, meaning it is in aperture.

24

Fig. 3.4 BGO PULSE HEIGHT ANALYZER

The output > L10 C indicates that electrons of energy higher than the defined upper limit (10 MeV incident) have been detected, since the output is that of a single comparator with threshold L10. This channel also detects in-aperture protons with energy greater than 270 MeV. The output > L10s does not require strobing with the coincidence pulses and is present whenever electrons or protons deposit more than $\simeq$ 10 MeV in the BGO crystal. Output pulses from the 10 energy bins and the 2 energy thresholds are counted by 12 counters.

3.7 Compression Counters and Shift Registers

The array of 22 counters in Fig. 3.1 is of the binary type. A mix of ripple and compression counters is employed. Compression counters are used here for the higher count rate channels to obtain good resolution while conserving telemetry resources.

Figure 3.5 shows, as an example, a 3 x 6 compression counter. The 6 bits of the mantissa are denoted as m_0 through m_5 and the 3 bits of the exponent as e_0, e_1, e_2 at the output of the compression counter. Assuming all counters are reset to $\emptyset$ by a RESET pulse, the first 63 counts are applied directly to the output counter via Q_1 of the input counter and the output of the multiplexer. However, at count 32, m_5 (MSB) is latched to a "1" by the S/R flip flop and the output counter is <u>reset</u> to $\emptyset$. Thus, for the first 63 counts the exponent remains $\emptyset$ and the counter counts by 1's. On count 64, e_0 goes high which steps the multiplexer to Q_2 of the input counter, causing the output counter to count by 2's. The exponent is now decimal 1 and m_5 (MSB of mantissa) remains high equivalent to decimal 32. Thereafter, the mantissa cycles between state 32 and 63, incrementing the exponent and dividing the previous count rate by 2 at each transition of the mantissa from state 63 to state 32.

The generalized expression for the total count N of a compression counter is given by

$$N = M \times 2^E$$

where M is the decimal value of the mantissa bits and E is the decimal value of the exponent bits.

The maximum count rates listed in Table 2.5 are the basis for assigning compression counters of various capacity to the several data channels. The selection is based on a 264-bit data readout every .512 second, and that the 264 bits must include 3 bits for the mode configuration and 8 bits for the PMT HV readout. This leaves 253 bits to be assigned to 22 compression counters. The estimated maximum counts and the compression counter assignments are given in Table 3.1. The design provides a minimum safety factor of 3 except for the 10^5 count channels (W_1 and W_2). Five types of counters are used: straight 10 bit counters; straight 12

Fig. 3. 5. 8 x 8 Comprehensive Counter.

bit counters; 3 x 8 compression counters; 4 x 8 compression counters and 3 x 10 compression counters.

The Counter/Shift Register/Spacecraft interface can be described as follows. At the end of each data accumulation period all counters are disabled and their content parallel transferred to the shift registers. Thus the data from 22 counters with a total of 264 bits, including 3 bits for mode status and 8 bits for PMT HV monitor are transferred. The number of bits transferred is the same for the normal mode and the CAL modes. After the transfer is accomplished the counters are reset and enabled, thus beginning the next data accumulation interval. The 264 bits now contained in the shift registers are serially transferred to the spacecraft data processing system during the next data accumulation interval. The serial transfer of the data is synchronized to the spacecraft telemetry by virtue of the following spacecraft signals: Major and minor frame sync., read gate and clock.

Table 3.1

Estimated Maximum Channel Counts and Compression
Counter Assignment

Channel Designation	Estimated Max Cnts (.512 sec)	Compression Counter* (Exp x Mantissa)	Maximum Counts
$> S_2$, Front	5,500	3 x 8	32,767
$> S_1$, Front	5,500	3 x 8	32,767
W_1, Front	3×10^5	4 x 8	1,048,575
W_2, Front	3×10^5	4 x 8	1,048,575
$> S_2$, Back	1,600	3 x 8	32,767
$> S_1$, Back	1,600	3 x 8	32,767
W_1, Back	15,500	3 x 10	131,071
W_2, Back	15,500	3 x 10	131,071
$> L_{10}s$	38,000	3 x 10	131,071
$> L_{10}c$	38,000	3 x 10	131,071
$L_9 - L_{10}$	95	x 10	1,023
$L_8 - L_9$	100	x 10	1,023
$L_7 - L_8$	90	x 10	1,023
$L_6 - L_7$	230	x 10	1,023
$L_5 - L_6$	190	x 10	1,023
$L_4 - L_5$	250	x 10	1,023
$L_3 - L_4$	335	x 12	4,095
$L_2 - L_3$	<500	x 12	4,095
$L_1 - L_2$	<850	x 12	4,095
$LL - L_1$	1,750	x 12	4,095
Any BGO ($>$ LL)	42,000	3 x 10	131,071
Ls	2.9×10^5	4 x 8	1,048,575

*Counters with no exponents are straight ripple counters with no compression.

29

3.8 In-Flight Calibration

There are three basic in-flight calibration modes designed to check the solid state detectors, the BGO and the plastic shield independently. Logic gates are used to effect the three modes as shown in Fig. 3.1. In mode CRF (Coincidence Requirement, Front) a logic high state at the input of the 2 OR gates overrides the pulse signals W1 and W2 from the front SSD-PHA. Hence, no coincidence is required with the front SSD to perform pulse height analysis of the calibration source, or of the ambient particle fluxes. In a similar manner a logic high state at input CRB (Coincidence Requirement, Back) voids the coincidence requirement with the back SSD. In mode ACR (Anti-Coincidence Requirement) a logic low state at the input of the AND gate disables the anticoincidence pulses from the shield. The selection of one of the three basic modes thus serves to check proper operation of the 2 SSD's and the shield, including their associated electronics. With all three modes selected simultaneously, the proper operation of the BGO and its electronics can be checked with the aid of the calibration source. In addition, enabling CRF and CRB together removes all coincidence requirements and permits analysis of any charged particle which deposits sufficient energy in the BGO but not in the shield. This mode is helpful in evaluating the efficiency of the shield and in measuring "omnidirectional" flux. The basic three modes and any combination thereof is selected by ground command via the timing and control logic described in the next section.

3.9 System Timing and Control

The timing and control logic (Fig. 3.6) receives CLOCK, GATE and command signals from the spacecraft and generates from them all control signals required for enabling and resetting the counters as well as transferring the counter data to the storage/shift registers and from there to the spacecraft. This circuitry also receives the calibration commands ACR, CRF and CRB from the spacecraft and generates the operating mode control signals required by the OR and AND gates described above. After initiation by command of a calibration mode it can be maintained for any time period until an OFF command is transmitted to return the instrument to its normal data mode. A Power ON/OFF command is required to turn the instrument on or off via the control logic, which also generates a signal to assure data mode operation after power turn-on. This in effect is a redundant command for the ACR, CRF and CRB OFF commands. The spacecraft command for the PMT Control consists of an 8-bit serial data word, a clock signal and a gate pulse, requiring 3 command lines. These commands are processed by the timing and control circuit to generate a suitable control signal for the PMT H.V. supply.
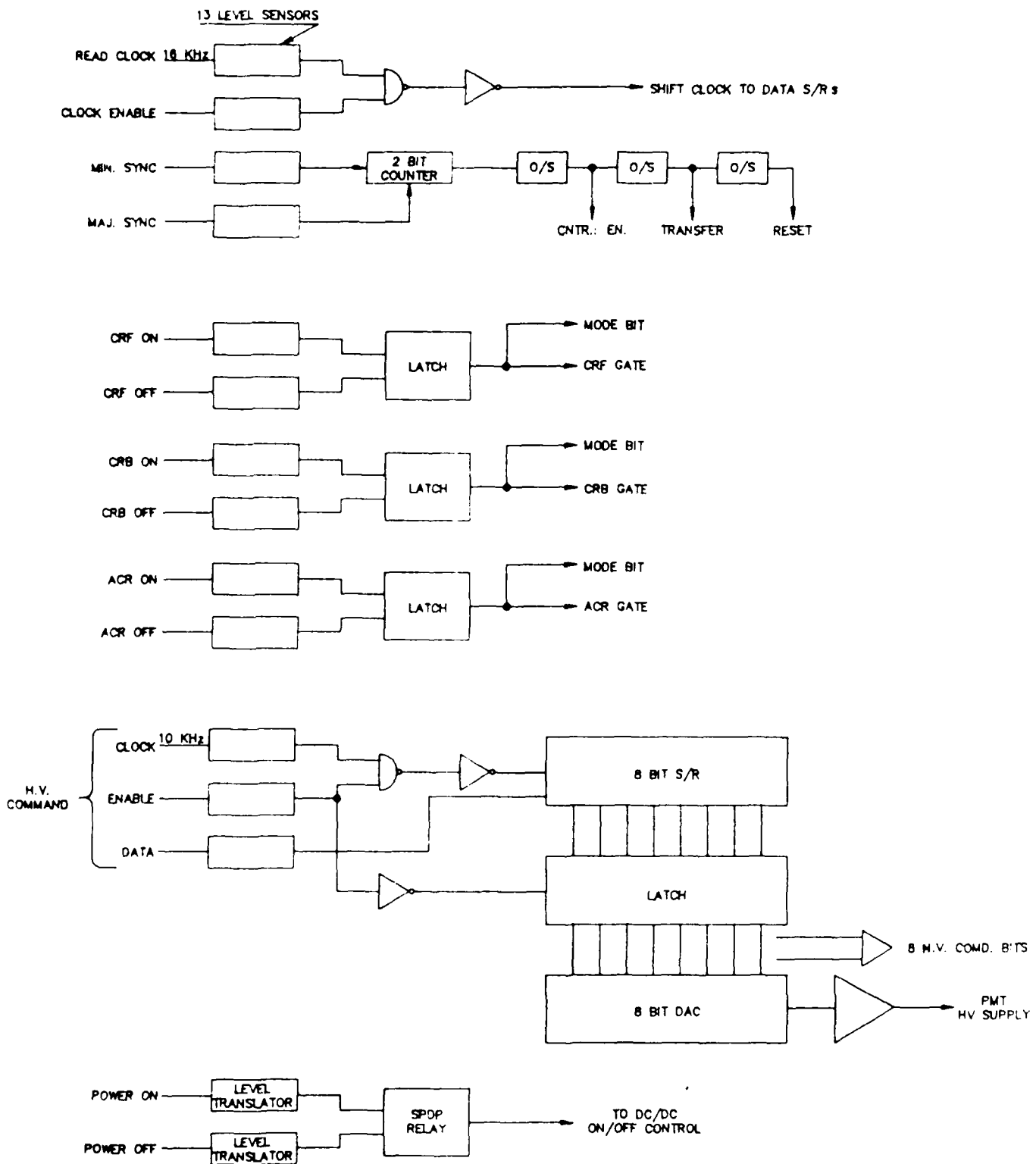
30

FIG. 3.6   SYSTEM TIMING AND CONTROL BLOCK DIAGRAM.

31

The timing and control logic provides an 11 bit output to the counter array in order to indicate the mode status (3 bits) and the PMT HV set point (8 bits) of the instrument. These bits are appended to the serial data stream from the shift registers and appear in every readout cycle. The modes indicated are: ACR - ON/OFF, CRF - ON/OFF and CRB - ON/OFF. The 8 H.V. set points indicate the current status of the H.V. Supply Command.

3.10 DC-DC Converter and Analog Monitors

Figure 3.7 shows the DC/DC converter and analog monitors in block diagram form. The converter consists of 3 sections: a low voltage and 2 high voltage (H.V.) converters. The low voltage converter is powered from the +28 V spacecraft buss through an EMI filter and a power switch. This power supply is turned on or off with a PWR ON/OFF Command supplied by the spacecraft telemetry. The low voltage outputs supply all necessary power to the analog and digital circuits. Analog monitors of these voltages are conditioned for telemetry purposes.

The SSD and PMT HV Converters receive their power from the regulated 12 volt output of the low voltage converter. Both are PWM converters of the flyback type and employ a Cockroft Walton voltage multiplier to generate the high voltage bias necessary. Low pass filtering in the output reduces the ripple to acceptable levels.

Additionally, the PMT H.V. bias is programmable with a suitable analog signal (Ref. V) applied. This signal is derived from spacecraft commands through the timing and control circuits as described in Section 3.9. Since the command consists of 8 binary bits, the programming reference voltage (Ref. V) can be incremented in 256 equal steps, corresponding to the same number of steps in the high voltage output. Choosing a value of approximately 1 V/step the high voltage bias for the PMT can thus be incremented over a range of $\pm$ 128 V. This range is large enough to correct for a 4x gain variations of the PMT due to temperature and aging.

Seven analog outputs serve to monitor all housekeeping functions, including temperatures of the Sensor and DPU.

4.0 INSTRUMENT DESCRIPTION

4.1 Physical Characteristics

The instrument consists of 2 subassemblies; the BGO Sensor and the Data Processing Unit (DPU) connected by an interface cable. Isometric views of the Sensor and DPU are shown in Figures 4.1 and 4.2, respectively.
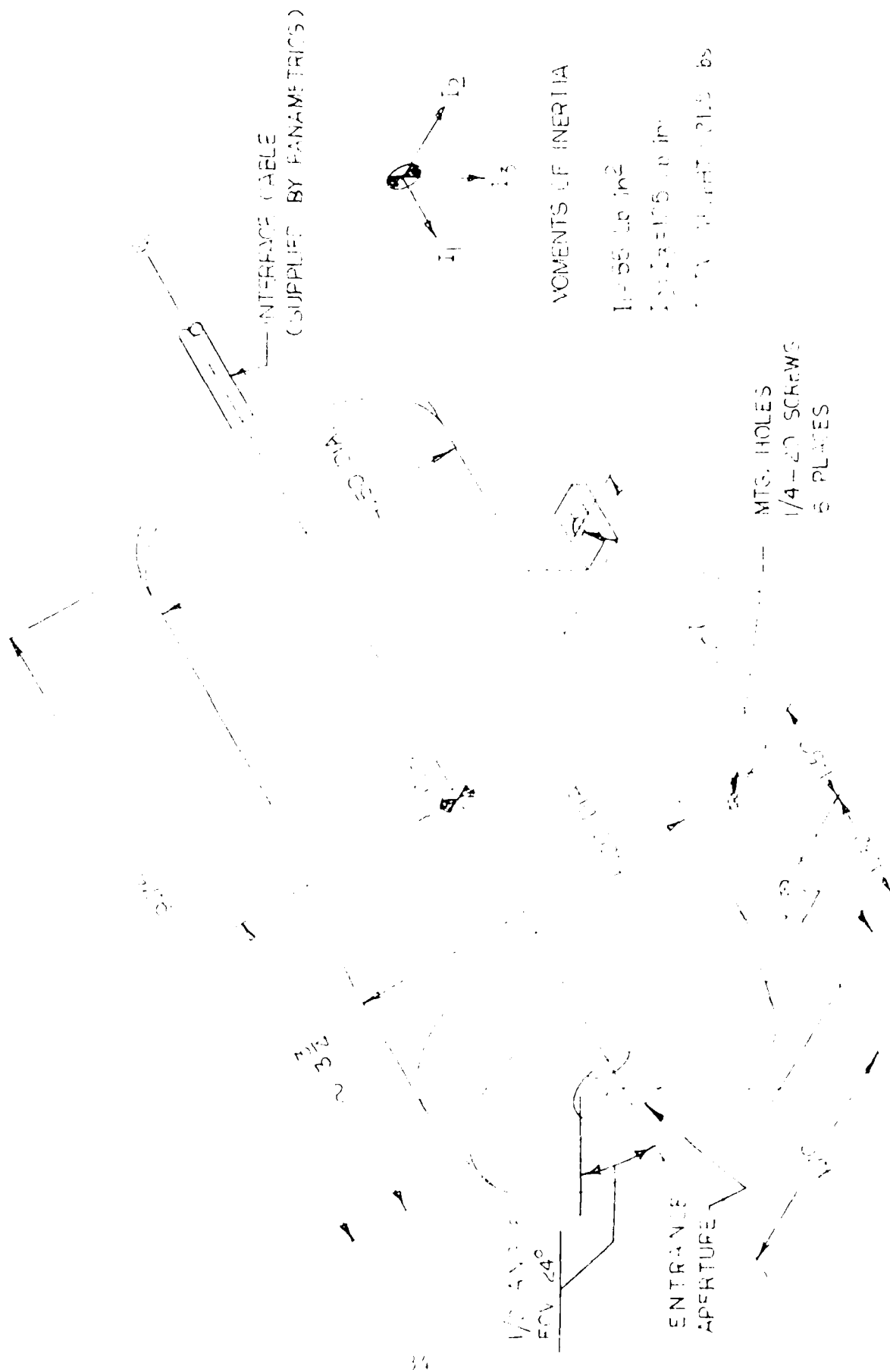
Low Voltage DC/DC Converter

SSD H.V. DC/DC Converter

PMT H.V. DC/DC Converter

PMT Filter

Power Switch

+15 V
+12 V
+10 V
+5 V
-5 V
Temp. Monitor, DPU
Temp. Monitor, Sensor
Low Voltage Monitors

SSD Bias
Bias Monitor

PMT Bias
PMT Monitor

ON/Pwr.OFF
Ref. V

From Timing & Control Logic

MOMENTS OF INERTIA

$I_1 = 35$ Lb in^2
$I_2 = 50$ Lb in^2
$I_3 = 53$ Lb in^2

TOTAL WEIGHT ≈ 6.5 Lbs

MTG HOLES
NO. 8 SCREWS
4 PLACES

MTG HOLES,
LOCATION

C.G.

SENSOR INTERFACE
CONNECTOR
15 PIN CANNON

TEST CONNECTOR
25 PIN CANNON

TELEMETRY INTERFACE, I/O CONNECTOR
25 PIN CANNON

Fig. 4.2 FLUXMETER, DATA PROCESSING UNIT (DPU) SUB-ASSEMBLY. PHYSICAL CONFIGURATION, C.G. AND MOMENTS OF INERTIA

35

The Sensor is further detailed in the cross sectional view given earlier in Fig. 2.1 It contains the BGO telescope (BGO crystal and 2 SSD's) the plastic scintillator shield, 3 PMT's, an HV supply and 4 Preamplifiers, one for each detector. PMT A is optically coupled to the crystal while PMT B and C are coupled to the plastic shield in diametrically opposed positions. A tungsten shield of approximately .200 in. thickness surrounds the detectors and 2 tungsten collimators of the same thickness are placed ahead of the front SSD. The telescope geometry defines a 7° acceptance half angle for high energy electrons. The housing for this subassembly measures approximately 9.75 in. x 5.20 in. at its largest diameter and consists of magnesium alloy for weight reduction with an electroless nickel finish.

The DPU contains all circuitry, except the preamplifiers, to process the Sensor signals and to interface with the spacecraft telemetry and power via the I/O connector. The telemetry signals include all commands, timing signals and the serial data stream from the DPU. The low voltage DC/DC converter is a subcontractor design. The DPU housing dimensions are 7.5 x 5.5 x 4.9 in. and the material used is 3/32 in. aluminum with a corrosion resistant finish. An additional paint finish is applied to 5 sides for thermal consideration while the bottom of the unit is unpainted.

The weight of the Sensor is 21 lb with a volume of 200 in.^{3}. The weight of the DPU is 5.8 lb with a volume of 200 in.^{3}. The total weight specification for the system is 27.5 lb with a total volume of 400 in.^{3}.

4.2 Electrical Interfaces

All electrical interfaces with the spacecraft are located in the Timing/Control circuitry while the power on/off interface is associated with the DC/DC converter. Connection to the interfaces is accomplished through the Telemetry Interface I/O connector. The pin assignment of this connector is shown in Table 4.1 and the interface circuits are shown in Figs. 4.3 and 4.4 for the AFGL-701-4 instrument.

The interfaces for science data counting, transferring and outputing to TM are based on the timing diagram for the CRRES vehicle and are shown in Fig. 4.5. The location of this data within each minor frame is depicted in Fig. 4.6. The words which contain 701-4 data are 26, 58, 90, 122, 154, 186, 218, and 250. In order to read out all data (264 bits) 4 consecutive minor frames must be scanned or a total of 36 words at 8 bits. Since this even multiple gives 288 bits it means that the last 3 words contain no information and can be discarded. In Table 3.1 the number of bits for each compression counter is given, which exceeds 8 bits in every case. Thus, the data read must take into account that the content of one counter is contained in more than one word.
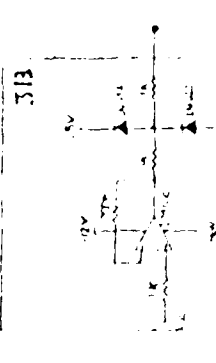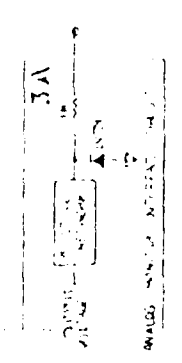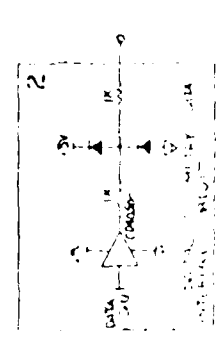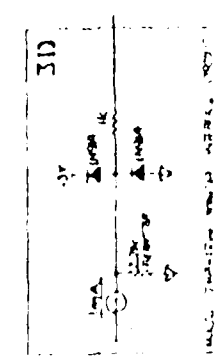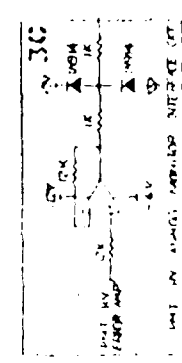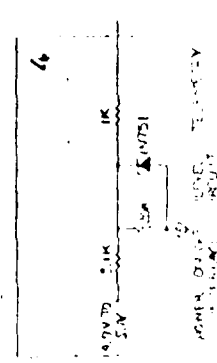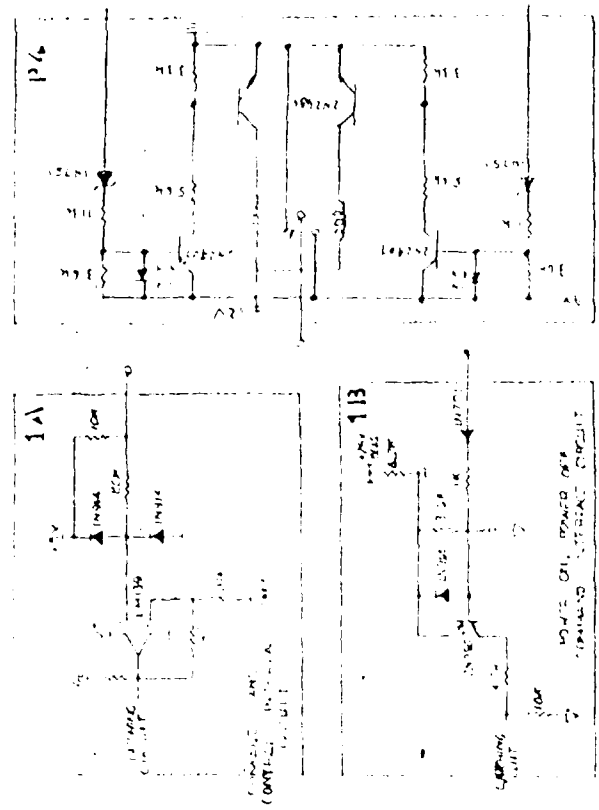
TABLE 4.1

CRRES FLUXMETER   (701-4)

CONNECTOR PIN ASSIGNMENT, Dwg. No. A-4831, Sheet 1   REV. A

P2, TELEMETRY INTERFACE I/O CONNECTOR, CANNON DDM-50P

Pin No	Function	Signal Type	Notes
1	Data	Serial Digital	NRZ
2	Signal Ground		
3	TLM Clock	16 kHz Digital Pulse Train	Open Collector
4	Clock Enable Gate	Pulse	Active Low
5	Major Frame Sync.	Pulse	
6	Minor Frame Sync.	Pulse	
7	N/C		
8	Serial Command	Serial Digital	16 bit command, 8 bits used
9	Command Clock	10 kHz Digital Pulse Train	
10	Command Enable Gate	Pulse	
11	CRF On	Low Level Discrete	Open Collector
12	CRF Off	"	Active Low
13	CRB On	"	
14	CRB Off	"	
15	ACR On	"	
16	ACR Off	"	
17-33	N/C		
34	Signal Ground		
35	Signal Ground		
36	Power On	Low Level Discrete	Open Collector
37	Power Off	Low Level Discrete	Active Low
38	+12, -6V Monitor	Analog	0-5.12 V
39	+16V Monitor	"	"
40	+10, +5V Monitor	"	"
41	PMT H.V. Monitor	"	"
42	SSD Bias Monitor	"	"
43	Temperature, Sensor	"	"
44	Temperature, DPU	"	"
45	DC/DC Alive Mon.	Bi-Level	
46	N/C		
47	+28V Return	Power Ground	Isolated from
48	+28V Return	Power Ground	Signal Ground
49	+28V Power	Buss Power	Continuous
50	+28V Power, Redundant	Redundant Buss Power	Continuous

Note: Signal Ground is internally connected to chassis inside the Sensor subassembly.
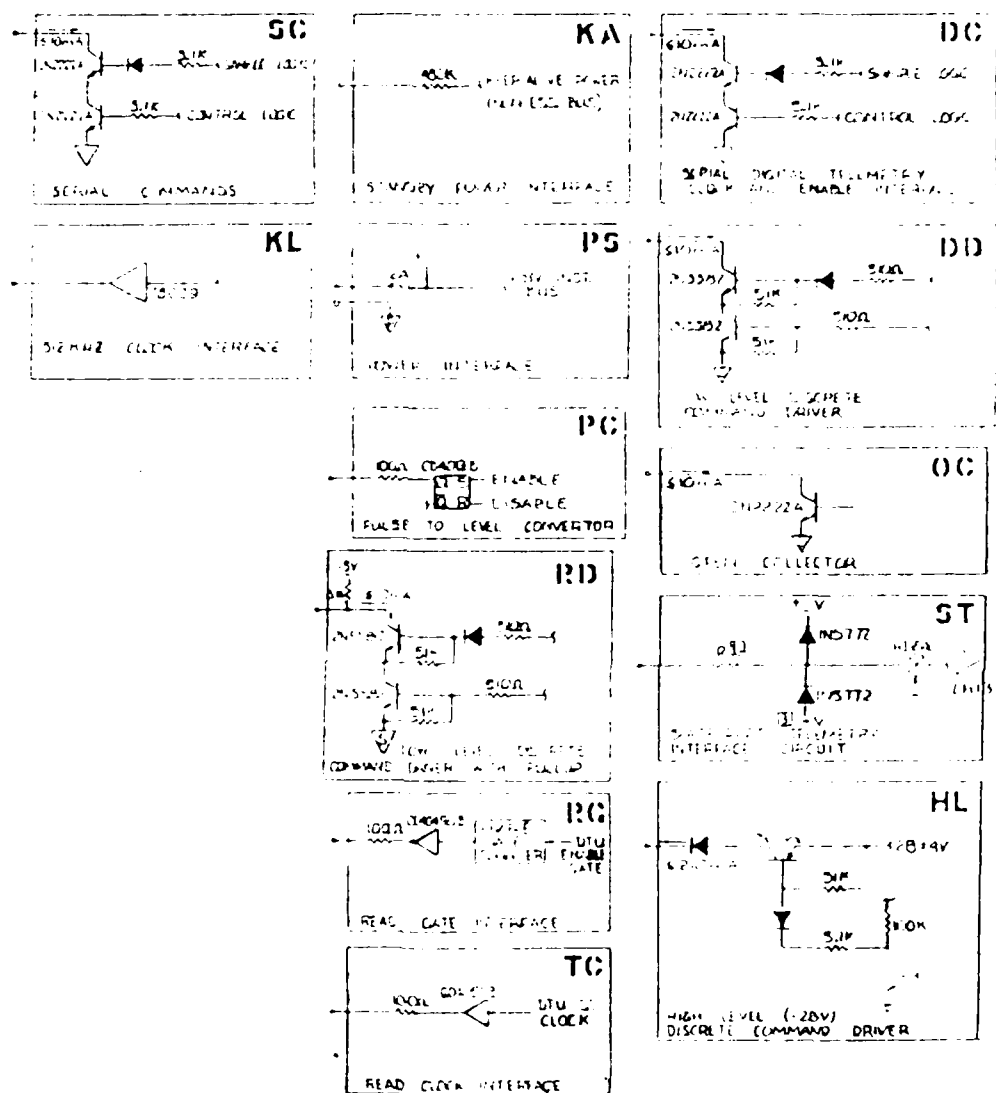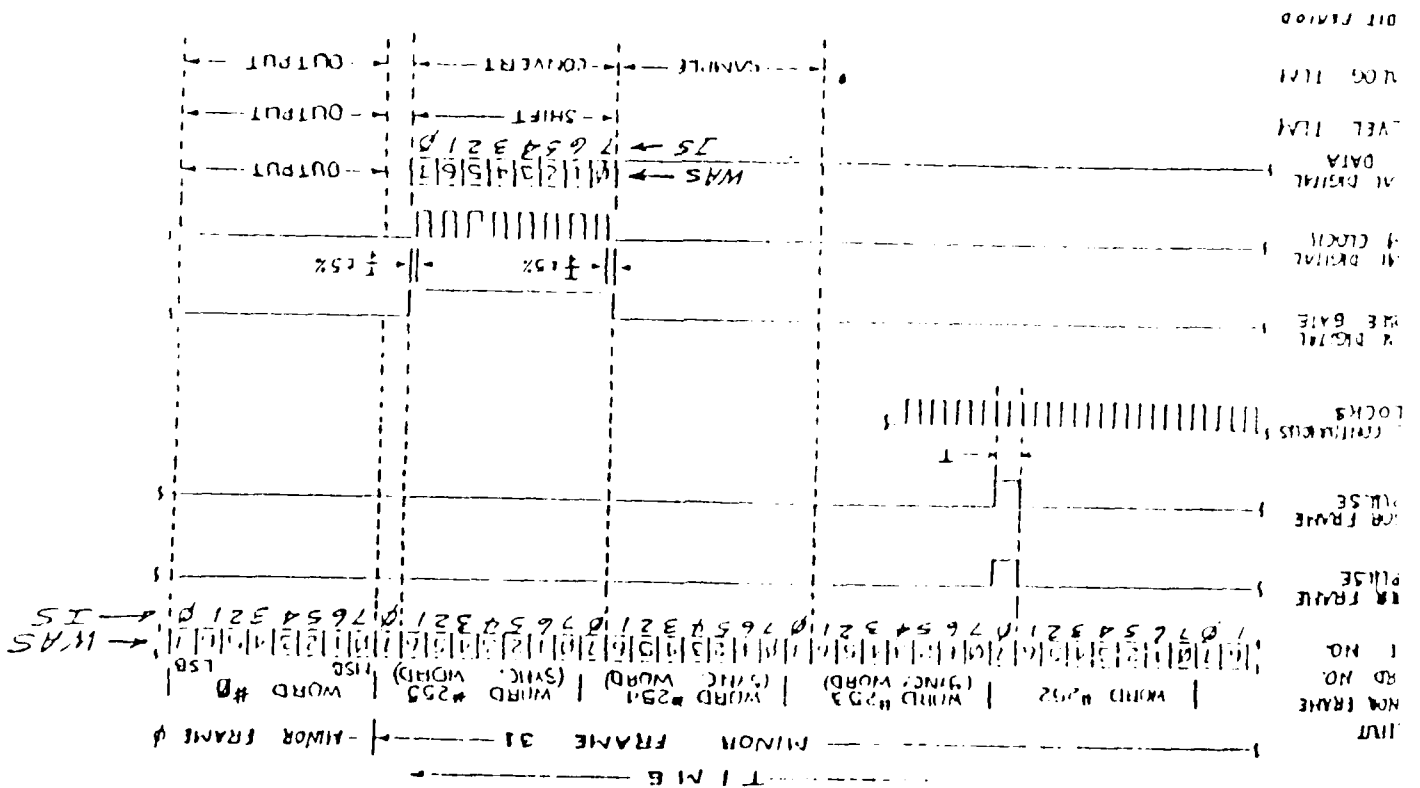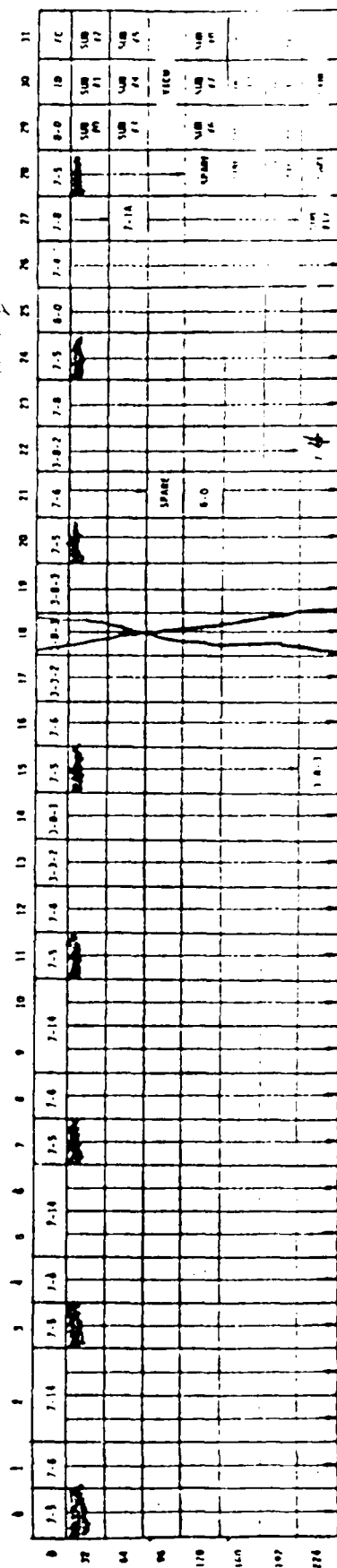
SPACECRAFT CIRCUITS

Fig. 4.4   AFGL-701-4   Interface Circuits

39

TELEMETRY FORMAT 2:GTO PHASE

1 Minor Frame

NOTES:

SPARE = UNASSIGNED WORD, 3 SPARE MINOR FRAME WORDS
VTCW = VEHICLE TIME CODE WORD
SYNC = FRAME SYNCHRONIZATION CODE
ID = DTU SOURCE ID (2 BITS), TLM FORMAT ID (2 BITS), BIT RATE ID (2 BITS), 2 BITS SPARE
FC = FRAME COUNTER
SUB #0 = 8 DEEP SUBCOM WITH ACCEPT CNTR A/B (2 WDS), REJECT CNTR A/B (2 WDS), BUS CURRENT (1 WD),
         CSM STAT. A/B (1 WD), 2 SPARE WDS

SUB #1
to SUB #14 = 32 DEEP SUBCOMS WITH S/C and INSTRUMENT ENGINEERING DATA

SUB #15 = 2 DEEP SUBCOM WITH AFGL-701-1B SCIENCE DATA (1 WD), 1 SPARE WORD
SUB #16 = 8 DEEP SUBCOM WITH AFGL-701-2 SCIENCE DATA (5 WDS), 3 SPARE WORDS
SUB #17 = 32 DEEP SUBCOM WITH ONR-307 STATUS DATA (18 WDS), 14 SPARE WORDS

Fig. 4.6 Word Allocation in One Minor Frame for AFGL-701-4

41

The last 11 bits of the serial data output indicate the status of the CRF, CRB and ACR commands and the 8 bits of the PMT HV command in that order. The last bit is the LSB of the HV command.

Once every major frame 7 analog signals and 1 bi-level signal are monitored. The analog signals are the +12V/-6V monitor, 16V monitor, +10/5V monitor, PMT HV monitor, SSD Bias monitor, the Sensor Temperature and the DPU temperature. The one bi-level signal monitors the power on/off condition.

The type command or signal and the sample rates are summarized in Table 4.2.

The power requirement of the Fluxmeter is 6W at 28V and requires a standby power of .28 W for the power on/off circuit.

4.3 Mechanical Interfaces

The outline drawing of the Sensor is shown in Fig. 4.7 and that for the DPU in Fig. 4.8. These drawings depict the mounting of the unit to the spacecraft shelf with insulators. Thus, the chassis of both units are isolated from the payload shelf. This was done to improve the signal to noise ratio especially for the SSD preamplifiers, since the low sides of their inputs are tied to the Sensor chassis.

The mounting configuration of the Sensor and DPU on the spacecraft is shown in Fig. 4.9. The Sensor location is indicated by view B-B and the DPU by view C-C.

The weight distribution is as follows:

Sensor	21 lb
DPU	5.8 lb
Total	26.8 lb

The specified weight limit is 27.5 lb.

4.4 Thermal Properties

The Fluxmeter is designed to operate over the operating temperature range -10° to $+40^\circ C$. The preferred operating range is 0° to $+30^\circ C$. The non-operating survival limits are from -25° to $+45^\circ C$. The thermal mass model for the two subassemblies is as follows:

Sensor	1000 cal/degree C
DPU	500 cal/degree C

Table ... Command and telemetry requirements

GTO INSTRUMENT - AIGL 701-4

SEQ NO	FUNCTION	COMMANDS			TELEMETRY				REMARKS
		HLIC	FLLDC	S/D	BLVL	ANA	S/D	SAMPLE RATE	
1	74 POWER ON		1						
2	74 POWER OFF		1						
3	74 PWR ON/OFF	1			1			.2441	
4	74 CRF ON		1						
5	74 CRF OFF		1						
6	74 CRB ON		1						
7	74 CRB OFF		1						
8	74 ACR ON		1						
9	74 ACR OFF		1						
10	74 CONFIG CONTROL			1					
11	74 +12,-6V MONITOR					1		.2441	8 BITS USED
12	74 +16V MONITOR					1		.2441	MAJOR FRAME
13	74 +10,+5V MONITOR					1		.2441	MAJOR FRAME
14	74 PMT H.V. MONITOR					1		.2441	MAJOR FRAME
15	74 SSD BIAS MONITOR					1		.2441	MAJOR FRAME
16	74 SENSOR TEMP					1		.2441	MAJOR FRAME
17	74 DPU TEMP					1		.2441	MAJOR FRAME
18	74 SCI DIGITAL DATA						1	10.3125	9 WORDS PER MINOR FRAME
	TOTALS		8	1	1	7	1		
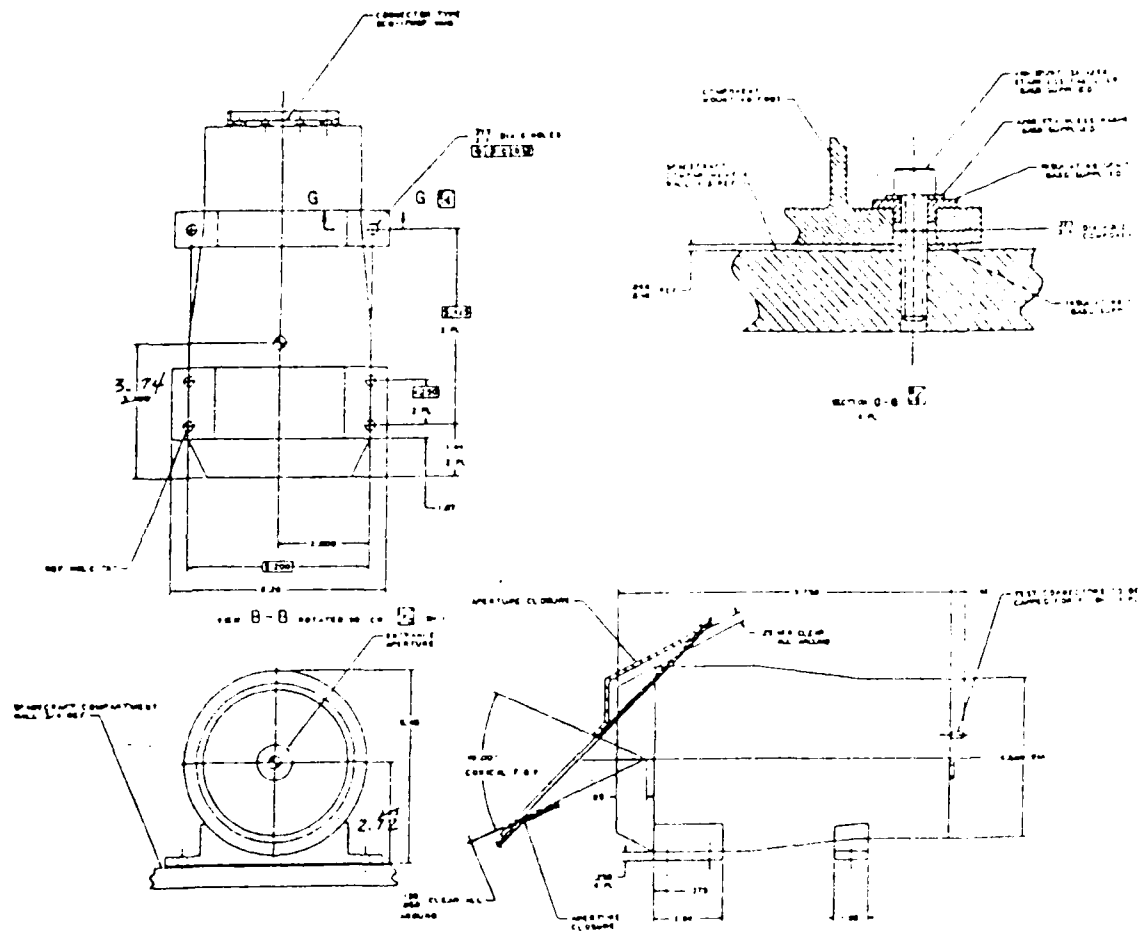
Fig. 4.7.   Outline and Mounting Detail of Sensor
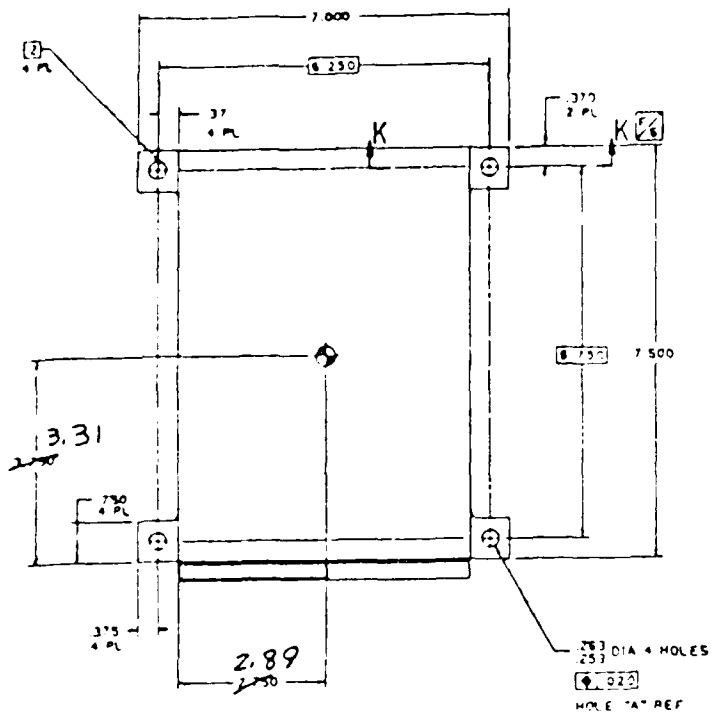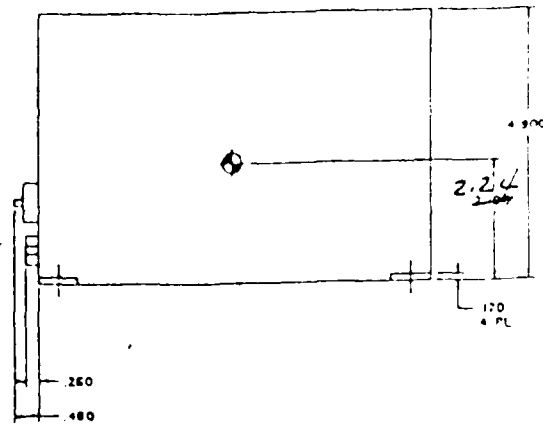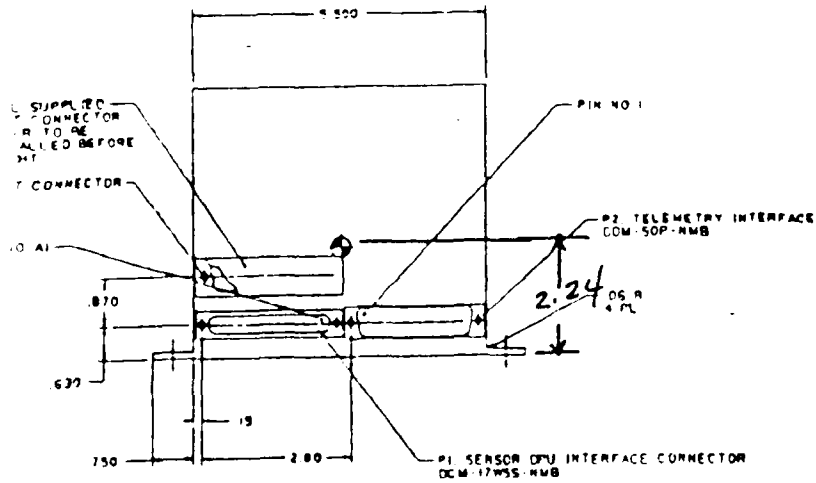
SECTION K-K
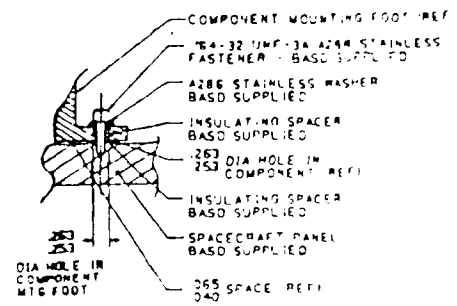
VIEW C-C ROTATED 180 SH I
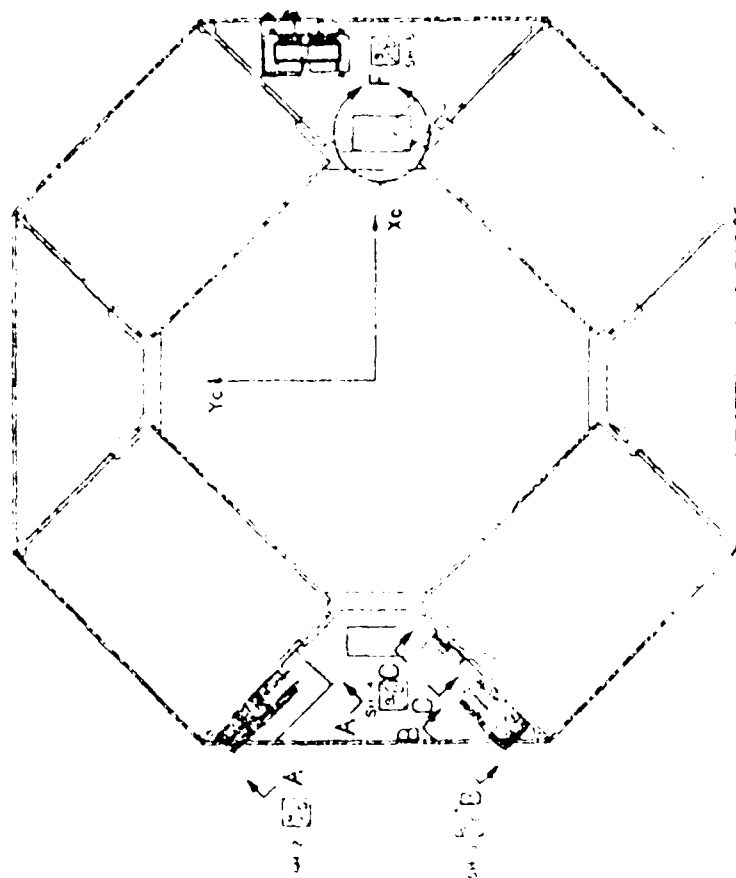ITEM #5 A464

Fig. 4.8 Outline and Mounting Detail of DPU

Fig. 4.9 Mounting Configuration of the Sensor
and DPU on the Spacecraft

5.0 Test and Calibration

5.1 Ground Support Equipment

Two separate units of GSE were designed and fabricated in order to perform the required acceptance tests of the instrument before delivery and for periodic checks during spacecraft integration. The two units are: 1) the spacecraft simulator and 2) the preamplifier buffer and driver unit. Additionally, test equipment for testing of each printed circuit board assembly was designed and fabricated. A total of 5 such units were required.

The spacecraft simulator consists of a Personal Computer (PC) fitted with a specially designed I/O extension board. The I/O board connects to the Fluxmeter telemetry interface connector with a 6 foot cable.

The PC in conjunction with its software simulates all spacecraft commands and provides for readout of digital data as well as analog and bi-level signals. The PC has the following capabilities with appropriate keyboard entries:

- a) Power ON/OFF command.
- b) Separate CRF, CRB and ACR ON or OFF commands.
- c) Selection of desired PMT HV from 1069 V in 25 increments to 1313 V. The nominal value being 1184 V at decimal command 128.
- d) Serial digital data read, display in decimal form for each energy channel and storage.
- e) Analog and bi-level signal read, display in appropriate engineering units and storage.
- f) Recording of all data on disc, if desired.

The second unit of test equipment is used primarily for initial calibration of the instrument with radiation sources. It is capable of driving 50 Ohm cables and returns the undistorted preamplifier signals with a gain of one. This unit connects to the test connectors on the rear of the Sensor housing with 4 short coaxes.

5.2 Instrument Tests

During the design phase extensive breadboard testing was carried out over the temperature range of -25° to $+50^\circ$C.

The flight unit was subjected to a complete series of functional and environmental tests as follows:

- a) Integration Tests including initial calibration with radiation sources.
- b) Thermal Engineering Test, -15° to $+40^\circ$C.
- c) Redundant Magnetic Field Measurements.
- d) Vibration and Shock Tests.
- e) Complete series of EMC Tests.
- f) Thermal Vacuum Tests, -10° to $+40^\circ$C.

g)   Thermal Cycle Test of 11 cycles.
h)   Final Performance Test.

The integration tests established the required gains of the four preamplifiers when irradiated with radiation sources of known peak energy. The thermal engineering test was carried out to assure that no anomalies occurred before the flight unit formal acceptance tests were started.

The vibration and shock tests were performed at the AFGL facilities. Pass/fail conditions were verified with pre and post performance tests. Each performance test is conducted per a written procedure which assures functional as well as performance adequacy to given test limits.

Certain of the EMC tests were done at Sanders Associates while others were performed at the Subcontractor facilities.

The thermal vacuum test consisted of the following sequence:

Performance Test at 25°c
12 hour non-operating soak at +40°C
Performance Test at +40°C
24 hour operating soak at 40°C
Performance Test at +40°C
12 hour non-operating soak at -10°C
Performance Test at -10°C
24 hour operating soak at -10°C
Performance Test at -10°C

The thermal cycle test consisted of 11 cycles with a dwell time of 2 hours at each temperature extreme. The temperature chamber set points were -20°C and +55°C. During each cycle the Sensor unit achieved -10°C and +30°C, while the DPU reached -32°C and +50°C. The temperature disparity between the 2 units is a consequence of their different mass.

The final performance test was carried out on 11/4/85. Subsequent to this date we were made aware by experiment scientists that failures of SSD's could occur if the SSD's are stored for a long period without a small bias voltage applied. Thus, AFGL requested addition of a battery powered bias supply incorporated in the flight unit. This request required design and fabrication of such a supply and installation in the flight Fluxmeter. After installation, the unit performance was verified by subjecting it to one thermal cycle. Delivery of the instrument occurred on 8/20/86.

5.3 Spacecraft Tests

After successful integration of the Fluxmeter on the CRRES spacecraft the following tests were performed at BASD in co-operation with subcontractor support personnel:

48

a) Magnetics Test
b) Low Frequency EMC Test
c) Integration Tests   - Isolation and Bonding
                        - Turn-On Surge
                        - Electrical Interfaces
                        - Performance Test
d) Baseline Performance Test
e) Functional Test
f) EMC Test
g) Thermal Vacuum Test

Note that more tests are still scheduled at BASD with subcontractor personnel participation. When all tests at BASD have been completed the instrument will be returned to the subcontractor for calibration at AFGL's LINAC and storage. New batteries for the SSD bias supply will be installed before final mounting on the CRRES spacecraft. This should occur as close to launch as possible.

5.4 Calibration

As mentioned above, the initial calibration was accomplished with radioactive sources. The solid state detectors and the plastic shield were calibrated with Cs-137 sources. The comptan edge having the energy of 478 keV was used. The BGO was also calibrated with Cs-137 sources, using the 662 keV gamma ray peak.

Tests at the Harvard Cyclotron served the purpose of verifying the instrument's rejection of protons from 15 MeV to about 140 MeV. This test was successfully conducted on 5/4 and 5/5/85. The in-aperture as well as the out-of-aperture response was tested.

A calibration with electrons from 450 keV to 1.8 MeV was conducted at the facilities of the Goddard Space Flight Center with good results.

6.0 INSTRUMENT OPERATION AND MAINTENANCE

For bench testing with the spacecraft simulator (Corona PC) a 28V P.S. of a 1.2A capability must be connected to the wire leads (red and black) attached to the PC extender board. The Fluxmeter is connected to the PC with a 50 pin connector and cable assembly. To operate the Fluxmeter the following sequence must be observed:

a) 28V PS OFF, PC OFF
b) Insert Program disc into drive A and the Fluxservice disc into drive B
c) Turn PC ON, input time and date
d) From keyboard type FLUX2, in DOS
e) After Prompt "__, type B
f) After B has been accessed the program Fluxservice must be removed

g)   Follow prompts on screen display which include instructions for initiating commands.

On the spacecraft the commands are applied to the Fluxmeter via the CRRES telemetry. A power ON command should only be sent in GTO.   This command also sets the CRF, CRB and ACR to the enabled state which is the normal data mode.   To obtain the various In-Flight calibration modes (discussed in Sec. 3.8), one, two, or all three coincidence/anticoincidence requirements must be commanded off.   After power-up the PMT HV comes on at its lowest voltage of 1069V. This voltage must be set to 1184V with a serial digital command equivalent of decimal 128.

The only maintenance requirement of the Fluxmeter concerns the battery for the SSD bias supply.   The batteries must be replaced every 2 years with 2 EVEREADY #350 cells in series if the instrument is stored in a non-operating condition.   This procedure will be followed when the instrument is returned after all spacecraft tests have been completed.

REFERENCES

1. M.J. Berger, and S.M. Seltzer, "Tables of Energy Losses and Ranges of Electrons and Positrons," NASA SP-3012 (1964).

2. M.J. Berger, and S.M. Seltzer, "Additional Stopping Power and Range Tables for Protons, Mesons, and Electrons," NASA SP-3036 (1966).

3. J.F. Janni, Calculations of Energy Loss, Range, Pathlength, Straggling, Multiple Scattering, and the Probability of Inelastic Nuclear Collisions for 0.1 to 1000 MeV Protons, AFWL-TR-65-150 (September 1966).

FILMED 58